Design and Validation of a Siphonic Hydropower Systems Tool

Undergraduate Honors Thesis

Presented in Partial Fulfillment of the Requirements for Graduation with Distinction in Mechanical Engineering of The Ohio State University

By

Simon F Conover

The Ohio State University

2021

Thesis Committee

Dr. Clarissa Belloni, Advisor

Dr. James Stagge

Abstract

Small hydropower (less than 30 MW) provides a path to adding power to the current energy infrastructure in a clean, renewable way. Further, since the available resource is consistent, it can supplement other forms of more intermittent green energy, such as wind and solar power. A large reason it is not implemented more broadly is its high initial costs, especially due to civil works during construction and installation. To mitigate this, small hydropower can be supplemented using siphonic hydropower with non-powered dams. Non-powered dams are structures already built over a waterway, primarily used for river control. By constructing a large siphon overtop of these dams and placing a reaction turbine in the middle of the piping, one can quickly, cost-effectively, and efficiently construct further hydropower schemes without the need for extensive civil works. Rickly Hydropower is a company building siphonic hydropower systems, however, they are in need of a tool to be used in the design phase for initial calculations. In this work, the construction and validation of a siphonic hydropower design tool in Microsoft Excel is explored. The tool uses certain inputs such as characteristics of the site, dimensions of the dam, material of the piping, and the flow rate through the turbine. In turn, the tool calculates various outputs, such as sizing (including length and diameter) of the piping to be used, pressure and cavitation concerns at several points, and the flow rate responses of the system. The developed tool was then validated through the construction of a scale model dam and siphon system within a flume on campus. Pressure values at two points of the siphon were found using manometers and compared to the predicted values initially produced by the tool. Results from this experiment will further confirm the efficacy of the tool, which will, in turn, aid in the design of these systems.

Acknowledgments

There are many people I would like to thank who have helped and supported me throughout my undergraduate research experience. Special thanks to Dr. Clarissa Belloni for advising me throughout the process and providing continual guidance. Thank you to Dr. Jim Stagge for use of the flume on campus used for the experimentation performed, and for serving on my thesis defense committee. Thank you to Mr. Kevin Wolfe in assisting in the machining operations for the dam and siphon system. Thanks as well to Mr. Ryan Cook and his colleagues at Rickly Hydropower for providing motivation behind the project itself, and for assisting in the design of the hydropower tool. Finally, thank you to all colleagues, peers, and friends who have helped along the way.

Table of Contents

List of Tables

List of Figures

Chapter 1: Introduction

This chapter introduces readers to the topic of small hydropower, and how siphonic hydropower can be used to more efficiently and cost effectively construct hydropower schemes. The section concludes with the objectives of this thesis, as well as a literature review of past studies on siphon hydropower design.

1.1 Small Hydropower

Throughout the nation today, electricity generation is currently dominated by fossil fuels. According to the US Energy Information Administration, in 2019 about 63% of the electricity generated in the United States came from fossil fuels, whereas 20% of energy came from nuclear sources, and only 18% came from renewable resources (US Energy Information Administration, 2021). With global warming on the rise, more energy needs to be produced from renewables. Small hydropower is one way to increase this generation of renewable energy.

The size of small hydropower is often defined differently between sources, however, for clarity in this report the US Department of Energy's definition is used. This source defines it as any type of hydropower project generating 10 MW or less of power at peak capacity (Water Power Technologies Office, n.d.). While these sites may not generate as much power as their large hydropower counterparts, they are enough to power a community nearby, and can supplement other forms of renewable power generation that may not be as consistent, such as wind and solar. Finally, if enough of these sites are constructed, they have the potential to add a significant amount of energy to the current grid.

This being said, constructing more hydropower plants come at a high expense – both monetarily and ethically. Hydro schemes come at a high up front cost, especially due to the

necessary damming of the river and other civil works that go into the construction. According to a report by the International Renewable Energy Agency, around 75% of the initial costs of constructing a hydropower project comes from these civil works (International Renewable Energy Agency, 2012). Furthermore, hydropower plants have the potential to ruin the surrounding ecosystem, displace many animals and wildlife, and – in the event of a collapse – could even destroy homes and communities.

This is where the perks of building on non-powered dams, or NPD's, can clearly be seen. NPD's are pre-existing dams constructed for a variety of purposes, including water supply and river control. As these dams already have the majority of the civil works performed, slight modification to fit a hydropower scheme is significantly more cost effective than constructing a small hydropower project from scratch. As well, a Department of Energy report has stated that there are at least 54,391 NPD's across the United States that are possible to be converted to a full hydropower scheme. These NPD's have the potential to add up to 12 GW of power to the grid, and could expand the existing hydropower fleet by 15% (Hadjerioua, Wei, & Kao, 2012).

1.2 Siphonic Hydropower

Siphonic Hydropower is one advantageous way to construct a hydropower scheme on a NPD. An image of this type of system, the PROPEL Hydro system, produced by Rickly Hydrological Company can be seen below, in Figure 1.

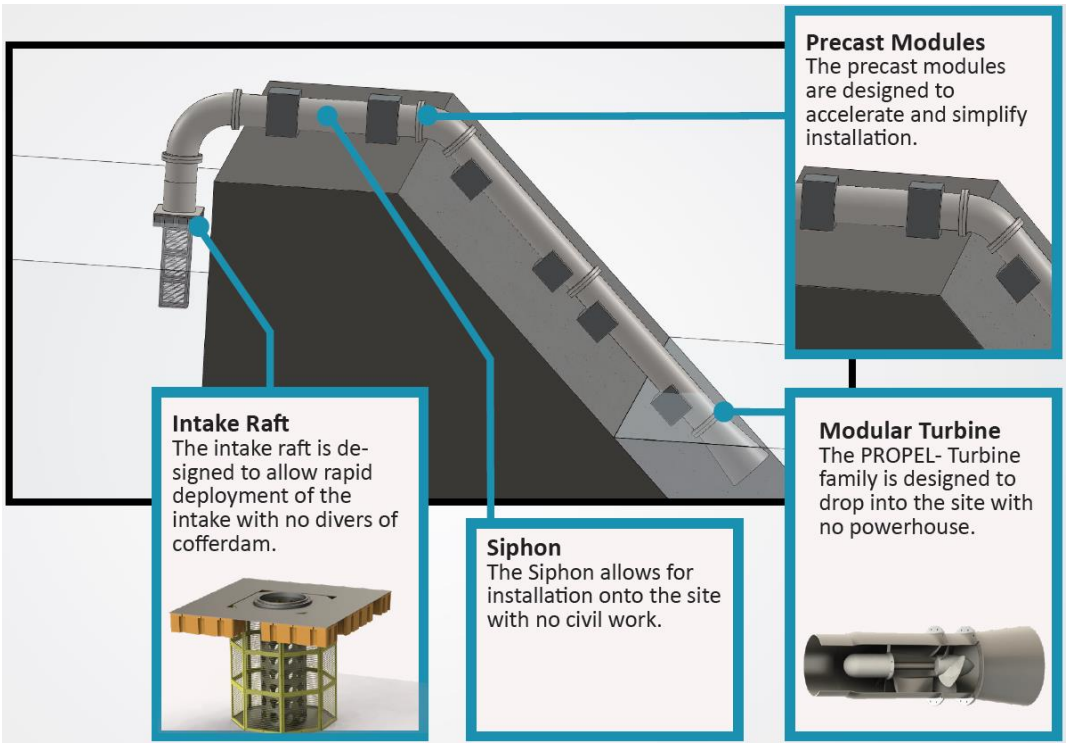

Figure 1: PROPEL Siphonic Hydropower System

Siphon hydropower is when a large siphon is constructed over top of a pre-existing dam, leading from the upper reservoir and into the lower reservoir. By adding a reaction turbine (a hydropower turbine driven by a pressure differential instead of impulse) at some point within the siphon, one is able to generate power quickly, cost-effectively, and efficiently. As well, Zhou et al., 2019 has shown that the efficiency of siphon hydropower projects have fared similarly to current hydropower projects – varying between 70% and 80%.

Despite the potential benefits, siphonic hydropower is not without its drawbacks. A majority of these problems are similar to any issue with hydropower projects, such as fish and debris finding its way into the system, as well as mechanical failure of various components. However, siphon hydro has other complications. This includes difficulty of start up and shut down of the siphon, as a majority of air needs to be removed from the system before the siphon activity can start. Due to this, siphon hydro often takes more time to initialize than a traditional hydropower

plant. As well, there is an added concern of cavitation within the system, as there are several points within the siphon itself that cavitation can occur due to the nature of siphonic activity.

1.3 Thesis Objectives

Rickly Hydro is a corporation that manufactures and installs several types of hydropower schemes. One of their schemes – the PROPEL-Hydro system – is a novel siphonic hydropower system which involves the use of several precast modules to be installed overtop a dam or weir, so installation cost and time can be decreased drastically. However, Rickly is in need of a tool to aid in several aspects of the initial design of these hydropower sites. The purpose of this research was to create and validate such a design tool. The tool would be designed using the following guidelines:

- The tool would take a variety of inputs including characteristics of the dam, atmospheric pressure and water temperature, flow rate of the turbine system, and pipe material.
- The tool would then calculate several outputs, including the length of the siphon, the diameter of the siphon, sizing of the intake, minimum depth the intake needs to be placed, maximum lift the siphon can achieve, and several cavitation concerns.

After this tool was created, several of the predicted values were validated against physical results. To achieve this purpose, a scale model siphonic hydropower system was constructed in a teaching flume on Campus. Pressure taps were placed at several points within the siphon, data of which was measured from a manometer and compared to the calculated values. Based on this validation, the design tool was adjusted accordingly.

1.4 Literature Review

A literature review was conducted on both numerical and experimental studies of siphons and siphonic hydropower to best appreciate the processes behind the systems and obtain an understanding of the variety of equations necessary for the design of the tool.

Potter & Barnes, 1971 discussed varying theories behind the inner workings of a siphon, initially considering several hydrostatic theories, then discussing a dynamic theory using an ideal, non-viscous liquid, and providing some modifications to take into account the viscous nature of liquids. These theories were then compared to experimental flow rate values found through siphons of varying sizes, where it was seen that the experimental values of the friction factor were higher than expected, and the values for the velocity head were lower than expected. This being said, part of the data collection method was flawed, as the flow rate collected was based on use of a plastic bin, and distances were simply measured using a meter ruler. The theories described by this paper were used as a basis for the siphonic theory discussed in section 2 below, and contained much of the motivation for several parts of the siphon design tool.

Kovari, 1984 discussed a variety of equations used when designing siphon systems, specifically within fish farms, including the characterization of flow rate, recommended pipe diameters, suction and downstream heads, and the necessary depth of the entrance to a siphon system. This being said, many of the equations detailed by Kovari were similar to derivations produced by Bernoulli's principle, but not exact, and neither the derivations nor references to where the formulae were derived were not included in the document. This being said, many of the safety factors described in this document were used throughout the construction of the siphon design tool.

Stark, Ando, & Hartley, 2010 created a complete parametric model of a siphon hydropower system, relating the electrical output power to the head and rotational speed of the turbine through a set of eight different equations. Values from this parametric model were compared to electrical results from an experimental hydropower system constructed within a flume. The researchers found high agreement between values generated from the parametric model and data obtained from the experimental system. Even so, much of the testing of the system was performed on a smaller sized flume, and as such many of the results may not be completely representative of a full scale siphon hydropower system. However, several elements within the testing setup were used as inspiration for the validation portion of this document, and the results further showed the efficacy of siphon hydropower systems.

Martinez et al., 2018 used a Sensory Fish, or a neutrally buoyant sensor instrument used to collect in situ force and motion data, to evaluate hydraulic characteristics with a siphon turbine system. This system was located in southern Idaho, contained an overall head of 5 m, and had a reaction turbine placed at the inlet of the siphon system. The hydraulic data collected was used to discuss fish mortality rates throughout a siphon hydropower system, and various design concerns and factors to mitigate these risks within siphon systems were suggested. This being said, the siphon fish only tested one siphon-hydro configuration – with the turbine system placed at the inlet – and other types of systems where the turbine was placed elsewhere was not considered. The pressure changes throughout the siphon seen by the sensor experimentally showcased – on a full scale siphon hydropower system – areas of interests to be understood within the design tool.

Zhou et Al., 2019 used a computational fluid dynamic (CFD) method to predict the hydraulic performance of an axial flow turbine, and verified the results using field test data. The data showed an efficiency of around 70% - 80% for these systems. A new siphon hydro turbine was

then proposed based on the CFD results. Similar to the work performed by Martinez et al., the CFD analysis only focused on one type of siphon hydro system, with the turbine at the inlet of the siphon. The efficiency found through the computational analysis further proved the efficacy of siphonic hydropower, and provided motivation for the construction of the design tool.

In summary, Potter & Barnes, 1971 discussed various theories in siphon operation and tested them through experimentation, however their data collection techniques were often flawed. The theories described were used as a basis for the siphonic theory discussed in section 2, and within the design tool. Kovari, 1984 discussed several recommended equations used for designing siphon systems, but did not include the derivations for these said equations. The factors of safety described within the equations were placed within the siphon design tool to construct the most conservative tool available. Stark, Ando, and Hartley, 2010, created a complete parametric model of a siphon hydropower system, and tested this model through the construction of a scale model system. This being said, the testing of the system was performed on a smaller sized flume, with many of the results not being completely representative of a full scale system. Several elements within the testing setup were used as inspiration for the validation portion of the document. Martinez et al., 2018, used a sensory instrument to collect in situ force and motion data through a siphon turbine system, however, only tested it on one siphon-hydro configuration. The pressure changes through the siphon experimentally showcased areas of concern within the design tool. Zhou et al., 2019 used a CFD method to predict the hydraulic performance of a siphon hydropower system, however, only tested this analysis on one configuration. The simulated efficiency proved the efficacy of siphonic hydropower, and provided further motivation for the work described throughout this document.

Chapter 2: Siphon Theory

This section provides the theory behind siphon operation, especially the variations in pressure throughout the siphonic flow. While the common concept of siphonic action includes the use of Bernoulli's principle alone, this case does not capture all aspects of flow through a siphon, as the fluid's viscosity and cohesive forces also play a large role (Potter & Barnes, 1971). The following sections explain the derivation of flow through a siphon using Bernoulli's principle, modifications to this derivation due to loss factors found in real fluids, and further contention to this theory based on the effects of viscosity and cohesive forces within fluids.

2.1: Siphonic Action Derivation Through Bernoulli's Principle

Considering an incompressible and non-viscous flow through a siphon, one may apply Bernoulli's principle. Referring to Figure 2, seen below, one can consider several points along the siphon and obtain an understanding of its operation. Within Figure 2 as well, the static gauge pressure based on Bernoulli's principle throughout the siphon is qualitatively shown and compared to points A through G in the graphic. While Bernoulli's principle does not initially incorporate friction losses, the graphic seen below does to better describe pressure seen within siphonic activity.

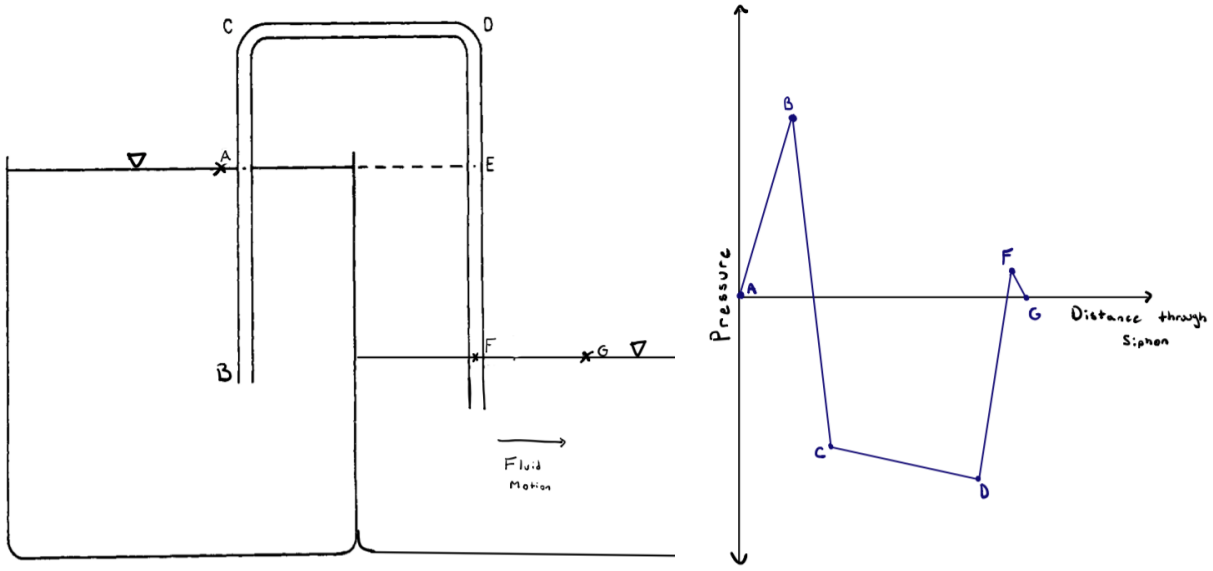

Figure 2: Siphon Model and Pressure Graph (Potter & Barnes, 1971)

Assuming that the reservoir in the image is large, the fluid in the upper reservoir at point A can be assumed to be motionless. As well, both points A and G are considered to be open to the atmosphere, and therefore their pressure is equal to one another. In addition, in this first equation, as said previously, no losses are considered throughout the piping. Taking this into account, Bernoulli's Principle applied from A-G (equation 1) is described through

$$P_A + \frac{1}{2}\rho v_A^2 + \rho g h_A = P_G + \frac{1}{2}\rho v_G^2 + \rho g h_G \quad (1)$$

And can be reduced to,

$$v_G^2 = 2g(h_A - h_G) \quad (2)$$

Where P is the static pressure of the fluid, v is the velocity of the fluid, h is the height of the fluid at each specified point measured from the base of the tank, ρ is the fluid density, and g is gravitational acceleration. Therefore, flow velocity through a siphon is directly related to the vertical distance between the upper reservoir and the exit of the siphon (Potter & Barnes, 1971).

As the flow through the siphon is compressible (even though flow speeds are low enough that the incompressible assumption can still be made) and viscous, several loss factors can be

implemented to more accurately predict the flow. These are described as major losses, which occur from skin friction drag along the surface of the pipe, and minor losses, which occur from flow passing through components in pipe systems. These losses can be implemented in the energy equation in the form of a loss in head. This energy equation can be considered an extension of Bernoulli's principle which itself is often described as the conservation of useful mechanical energy.

Major losses can be calculated from the overall length of the pipe section (l), the diameter of the pipe (D), velocity of the flow throughout the pipe (v), gravitational acceleration (g), and a friction factor (f). This friction factor is a function of the Reynolds number (Re), diameter of the pipe (D), and roughness in a pipe (ε), and can be calculated for turbulent flow from the Colebrook equation, seen below in equation 3. This equation is an empirical fit of pipe flow data, and can be solved implicitly. This can be placed into the overall major loss equation, seen in equation 4.

$$\frac{1}{\sqrt{f}} = -2.0 \log\left(\frac{\varepsilon/D}{3.7} + \frac{2.51}{Re\sqrt{f}}\right) \quad (3)$$

$$h_{L\,major} = f\frac{l}{D}\frac{v^2}{2g} \quad (4)$$

Where $h_{L\,Major}$ are the major losses of the system. The Reynolds number within this equation is a dimensionless value used to predict viscosity effects within flow – at low Reynolds (less than 2100), the flow within the pipe can be described as laminar, and the effect of viscosity is high. At high Reynolds numbers (greater than 4000) the flow within a pipe can be described as turbulent, and the effect of viscosity is low (Gerhart, Gerhart, & Hochstein, 2016). Laminar and turbulent flow can be described as qualitatively different. As well, the Reynolds number is calculated based on equation 5, seen below.

$$Re = \frac{\rho v L}{\mu} \quad (5)$$

Where ρ is the density of the fluid, v is the velocity of the fluid, μ is the dynamic viscosity of the fluid, and L is a critical dimension within the flow. For pipe flow, this dimension is the diameter of the piping. Minor losses are calculated from the velocity of the flow throughout the pipe (v), gravity (g), and a loss coefficient (K_L), which is dependent on the geometry of the pipe component considered and other fluid properties. The minor loss equation can be seen below, in equation 6.

$$h_{L\,minor} = K_L \frac{v^2}{2g} \quad (6)$$

With $h_{L\,minor}$ being the total minor losses of the system. These loss factors can be described as a loss in head, and can be implemented into equation 2 to form equation 8 (Gerhart, Gerhart, & Hochstein, 2016, pp. 427-441).

$$h_L = h_{L\,minor} + h_{L\,major} \quad (7)$$

$$v_F^2 = 2g(h_A - h_G - h_L) \quad (8)$$

As well, pressure concerns can be made very apparent at several points within the siphon. As was demonstrated through Bernoulli's principle above, the pressure within the siphon above the upper reservoir must be lower than atmospheric pressure for siphonic action to occur. After the fluid drops below the upper reservoir water level, it may either be above or below atmospheric depending on the flow rate. Within Figure 2, one can see that the lowest pressure in the siphon will occur at point D, as this location is the highest above the upper reservoir's surface. The pressure at this point can be found based on application of Bernoulli's equation from station A to D.

$$P_D = P_A + \rho g(h_A - h_D) - \frac{1}{2}\rho v_D^2 - \rho g h_L \quad (9)$$

If the absolute pressure at this point were to drop below vapor pressure, the fluid would cavitate and siphonic activity would stop. In addition, the pressure head at this point must be greater than the upstream head of the site, or the fluid will not be able to flow up the intake of the siphon.

As well, a second point of concern is the end of the siphon, prior to the fluid entering into the lower reservoir. This can be seen as point F in Figure 2. At this point, overall losses will be the greatest throughout the siphon as a whole, and there is a chance of the siphon cavitating if these losses cause the pressure to drop below the vapor pressure. The pressure head at this point must also be greater than the overall head of the site, or cavitation can occur as well. The pressure at this point can be calculated based on an application of Bernoulli's principle from station A to F, seen in equation 10 below.

$$P_F = P_A + \rho g(h_A - h_F) - \frac{1}{2}\rho v_F^2 - \rho g h_L \qquad (10)$$

The priming of a large siphon is somewhat difficult, as the pressure throughout much of the volume within the siphon must be below atmospheric for the siphon to run. Traditionally siphons are primed by enabling a vacuum pump to suck enough air from the pipe that water will eventually flow through the down leg of the siphon. In addition, once the pipe flows full (at around 7 ft/s), the large siphon can run on its own without the need of a vacuum pump, but average velocity within must remain above 5 ft/s to adequately purge entrained air, as is stated by recommendations from the URS Corporation (URS Corporation, 2010). A secondary method can also be used by incorporating a water pump instead of a vacuum pump. In this method, a valve at the end of the siphon is closed, and a water pump is used to pump water into the down leg of the siphon. Once this is filled the valve is opened again, and the subsequent vacuum left by

the water leaving the down leg flushes the air out of the remainder of the siphon and forces siphonic activity to begin.

2.2: Viscous Effects

Several studies have shown that a fluid's viscosity and cohesive forces play a large role in the activity of a siphon. As was demonstrated above in equation 9, the lowest pressure in the siphon occurs at point D, and is directly related to the difference in height between the upper reservoir and top of the siphon, fluid velocity, and head losses. Theoretically the maximum height a siphon can reach is directly related to this height difference and the available atmospheric pressure at the location. However, others have discussed that siphons may be driven to lengths greater than what was previously thought. For example, Potter and Barnes have discussed that mercury siphons can reach maximum heights larger than what is theoretically possible (Potter & Barnes, 1971). This shows that while atmospheric pressure of the location and the height difference between points still play a large role in siphonic activity, cohesive forces and fluid viscosity are a large factor as well, and can push siphon operation past the theoretical maximum limits set by Bernoulli's principle. To construct the most conservative tool for use by Rickly Hydropower, viscosity effects of water have been neglected throughout the tool, and equations for use have been described by Bernoulli's principle alone.

Chapter 3: Design of a Siphonic Hydropower Tool

Throughout the course of this next section, the design and assembly of the siphon hydro tool in excel will be discussed. The subsections are broken down from each separate excel tab of calculations within the design tool, beginning with the input to the design tool, and following with the pre-diameter, diameter, and post diameter calculations. Next, the pressure and volume flow calculations are discussed, and the section will conclude with the siphon design tool output.

3.1 Input

The input to the design tool was largely based on recommendations provided by Rickly Hydro, who had explained that they would be able to provide the volume flow of the siphon system, technical inputs to the siphonic flow – such as atmospheric pressure – and the general configuration of the siphon itself. These values were used throughout the rest of the design tool itself for the variety of calculations performed. As well, a rudimentary design tool used by Rickly to calculate loss factors was reviewed to gain further information. Based on this knowledge, the input was created, and can be seen below in Figure 3.

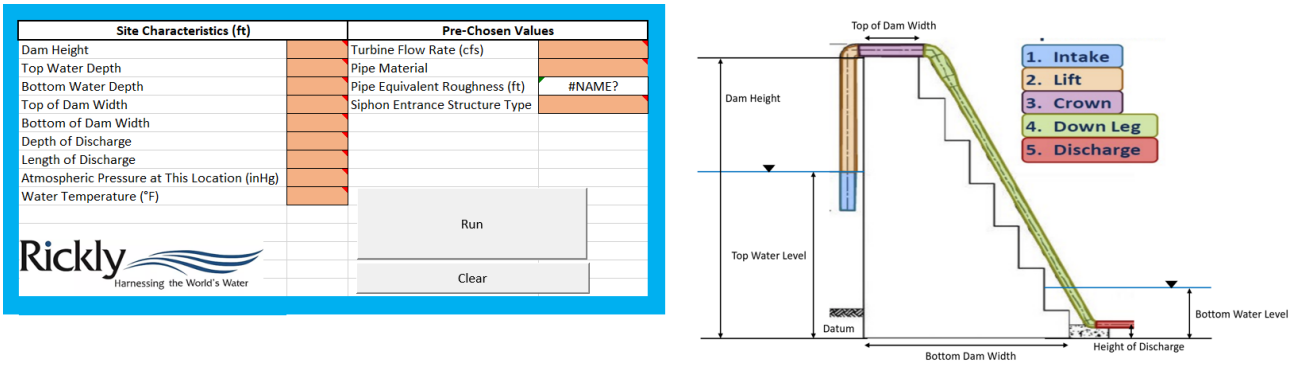

Figure 3: Input to Siphon Design Tool

As one can see, the input is broken down into two major sections – site characteristics and pre-chosen values. The site characteristics are physical characteristics of the dam itself. These included the overall height of the dam (measured from the base of the dam to its peak), the

water depth of the upper reservoir, the water depth of the lower reservoir, the width of the top of the dam (measured between the upper and lower reservoirs), the width of the bottom of the dam (measured between the upper and lower reservoirs), the length and depth of the discharge of the siphon, and the atmospheric pressure and water temperature of the location.

The pre-chosen values used included the flow rate of the siphon system itself in cubic feet per second, the material of the piping used, and the entrance type of the siphon (A, B, or C). The material used can be selected from a drop down list, and was necessary in finding the equivalent roughness of the siphon system. The siphon entrance type was based on three different sized siphon entrances that Rickly produces as a part of its PROPEL siphon-hydro system, and were used to calculate the length of the intake.

To further clarify the dimensions provided by the user, a diagram was created based on an illustration previously provided by Rickly used in the design of their siphon systems. This diagram can be seen below, as Figure 4. As well, hints were provided for the user in the necessary cells where values needed to be placed.

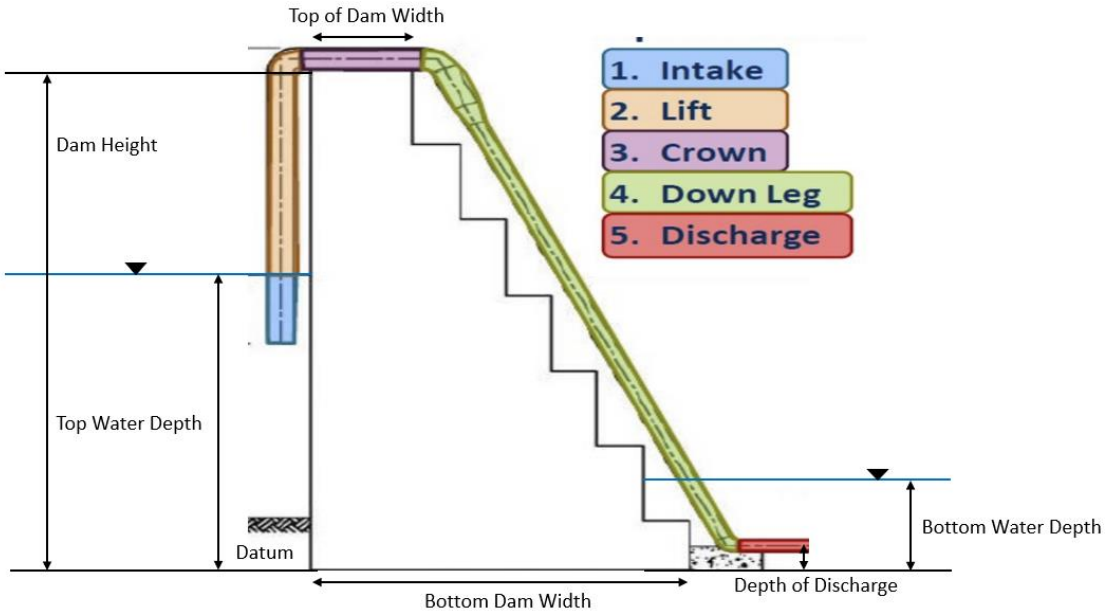

Figure 4: Siphon Component Diagram

3.2 Pre – Diameter

As the calculations to find the diameter itself needed several preliminary values, these were calculated in their own separate tab. This tab can be seen below, in Figure 5.

Converted Values				Water Properties Table			
Flow Rate (m^3)	0.000764108			Temp (C	Dynamic Viscosity (N*s/m^	Density (kg/m^3	Vapor Pressure (Pa)
Roughness (m)	4.57317E-05			10	1.31E-03	999.7	1.23E+03
Water Temperature (°C)	-7.22222222			20	1.00E-03	998.2	2.34E+03
Atmospheric Pressure (Pa)	101354.6527			30	7.98E-04	995.7	4.24E+03
				40	6.53E-04	992.2	7.38E+03
Siphon Lengths (m)							
Safety Factor to Increase Leng	1.1						
Intake	1.9558						
Lift	0.012573						
Crown	0.090804888						
Down Leg	0.502969188						
Discharge	0						
TOTAL LENGTH	2.562147076						
Water Properties							
Dynamic Viscosity (N*s/m^2)	0.001307						
Density (kg/m^3)	999.7						
Vapor Pressure (Pa)	1228						
Minor Loss Coefficients (-)							
Entrance Loss Coefficient	0.8						
Exit Loss Coefficient	1						
90° Turn (Flanged)	0.3						
45° Turn (Flanged)	0.2						
UPSTREAM LOSS COEF SUM	1.1						
DOWNSTREAM LOSS COEF SUM	1.2						
Local Loss Coefficient Sum	2.3						

Figure 5: Pre-Diameter Tab

First, the all previous values obtained from the input were converted to metric units as some of the semi-empirical formula used within the design tool utilized these units. The lengths

of each respective leg of the siphon were calculated based on the dimensions of the dam itself, and were increased by 10% to account for variability when constructing the physical system. This extra 10% added to the system makes the calculations further conservative, as an increased length of piping adds more losses to the system. The water properties were found based on the previously selected temperature, whose values were found within Munson's Fundamentals of Fluid Mechanics (Gerhart, Gerhart, & Hochstein, 2016). Certain minor loss coefficients were selected based on further discussion with Rickly Hydro in what was included in their siphon systems.

3.3 Diameter

The appropriate diameter for use within the siphon system was found based on variations of loss factors and velocity throughout the siphon. The cost of piping is roughly correlated to its diameter size – a larger sized pipe is more expensive to purchase, is more difficult to transport, needs larger supports, among other aspects – therefore, the smallest possible pipe diameter should theoretically be used (Nevers, 1991, pp. 218-221). However, this size is limited by the pressure of the siphon itself, as a smaller sized diameter will allow for a larger fluid velocity, incur greater friction losses, and thereby allow for a lower total pressure throughout the siphon. As was stated in the section 2, the point where the lowest amount of pressure would occur is at the upper most location in the siphon prior to the down leg, or seen as point D in Figure 2. Therefore, the smallest pipe diameter size should be used without cavitation occurring at this point. The tab where the diameter was calculated can be seen below, in Figure 6. Due to sizing constraints the tab itself was split in two, where the velocity head column would directly follow the friction factor column.

Initial Values			Diameter (m)	Area	Velocity	Reynolds Number	Relative Roughness	Friction Factor
Turbine Flow Rate (m^3/s)	0.000764108		0.01	7.85E-05	9.7289281	74414.76223	0.004573171	0.03088065
Density (kg/m^3)	999.7		0.02	0.000314	2.43223203	37207.38111	0.002286585	0.027949712
Dynamic Viscosity (N*s/m^2)	0.001307		0.03	0.000707	1.08099201	24804.92074	0.00152439	0.027918639
Roughness (m)	4.57317E-05		0.04	0.001257	0.60805801	18603.69056	0.001143293	0.028611
Atmospheric Pressure Head (m)	10.33486934		0.05	0.001963	0.38915712	14882.95245	0.000914634	0.029512758
Top Water Level (m)	0.35052		0.06	0.002827	0.270248	12402.46037	0.000762195	0.030463538
Dam Total Height (m)	0.36195		0.07	0.003848	0.19854955	10630.68032	0.00065331	0.031406969
Initial Lengths (m)	2.059177888		0.08	0.005027	0.1520145	9301.845279	0.000571646	0.032322683
Vapor Pressure Head (m)	0.125215954		0.09	0.006362	0.12011022	8268.306914	0.00050813	0.033204104
			0.1	0.007854	0.09728928	7441.476223	0.000457317	0.034050237
Diameter Calculations			0.11	0.009503	0.08040436	6764.978385	0.000415743	0.03486236
Allowable Pressure Head (m)	1.125215954		0.12	0.01131	0.067562	6201.230186	0.000381098	0.035642613
Selected Diameter (m)	0.02		0.13	0.013273	0.05756762	5724.212479	0.000351782	0.036393378
			0.14	0.015394	0.04963739	5315.340159	0.000326655	0.037117001
SELECTED COMMERCIAL PIPE (in)	1		0.15	0.017671	0.04323968	4960.984149	0.000304878	0.037815685
			0.16	0.020106	0.03800363	4650.922639	0.000285823	0.03849144
$\frac{1}{\sqrt{f}} = -2log_{10}\left(\frac{\varepsilon}{3.7D_h} + \frac{2.51}{Re\sqrt{f}}\right)$	Colebrook Equation		0.17	0.022698	0.03366411	4377.338955	0.00026901	0.039146083
			0.18	0.025447	0.03002756	4134.153457	0.000254065	0.039781246

Velocity Head	Upstream Minor Losse	Upstream Major Losses	Pressure Head at Top of Siphon (m)	Commercially Available Pipe Diameters	
				Imperial Units (in)	Standard Units
4.824263099	5.306689409	0.148976379	-0.989976482	0.5	0.0127
0.301516444	0.331668088	0.008427298	8.648340576	0.75	0.01905
0.059558804	0.065514684	0.001662801	9.163216117	1	0.0254
0.018844778	0.020729256	0.000539168	9.249839204	1.25	0.03175
0.007718821	0.008490703	0.000227804	9.273515078	1.5	0.0381
0.003722425	0.004094668	0.000113398	9.282021914	2	0.0508
0.002009272	0.0022102	6.31052E-05	9.285669828	2.5	0.0635
0.001177799	0.001295578	3.80696E-05	9.287440959	3	0.0762
0.000735294	0.000808823	2.44148E-05	9.288383874	3.5	0.0889
0.000482426	0.000530669	1.64267E-05	9.288922884	4	0.1016
0.000329504	0.000362454	1.14873E-05	9.289248961	5	0.127
0.000232652	0.000255917	8.29231E-06	9.289455545	6	0.1524
0.000168911	0.000185802	6.14724E-06	9.289591546	8	0.2032
0.00012558	0.000138137	4.66114E-06	9.289684027	10	0.254
9.52941E-05	0.000104823	3.60361E-06	9.289748684	12	0.3048
7.36124E-05	8.09737E-05	2.83345E-06	9.289794986	14	0.3556
5.77611E-05	6.35372E-05	2.26112E-06	9.289828846	16	0.4064
4.59559E-05	5.05515E-05	1.82818E-06	9.28985407	18	0.4572
3.70183E-05	4.07201E-05	1.49548E-06	9.289873172		

Figure 6: Diameter Tab

Similar to the pre-diameter tab, various initial values used in the calculations of the diameter were imported from the input and pre-diameter tabs, including turbine flow rate, water density, dynamic viscosity, surface roughness, the atmospheric and vapor pressure heads, and dimensions of the dam itself. Based on this information, pipe cross sectional areas and velocity values for diameters ranging between 0.01 m to 2.5 m were calculated. According to this, subsequent Reynolds numbers and relative roughness values were also found. The friction factor was then calculated for each diameter value based on the Colebrook equation, as well as the subsequent major and minor pipe losses up to the critical pressure location near the crest of the siphon.

Finally, the pressure head at this pipe location was calculated for every diameter within the provided range.

Next, an allowable pressure head was found for which to compare to. This consisted of the vapor pressure head of water at the location temperature and pressure, with a safety factor of 1 meter added in accordance with siphon guidelines set by the Food and Agriculture Organization of the United Nations (Kovari, 1984). A graph with a variation in pressure heads against the allowable pressure can be seen below, in Figure 7.

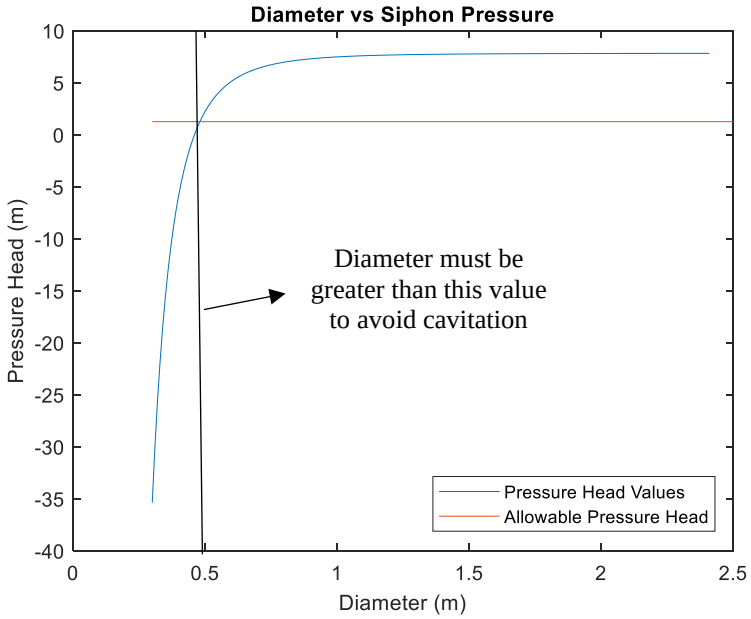

Figure 7: Diameter Compared to Siphon Pressure at Crest

At the intersection of these two curves, an appropriately sized diameter should be used. An excel INDEX-MATCH function was subsequently used to compare the allowable pressure head to the range of pressure heads at the top of the siphon, and select the pipe diameter which best matched the two values. This selected pipe diameter was then compared to a list of commercially available pipe diameters using a second INDEX-MATCH function to find the best pipe available for purchase. To provide the most conservative tool for use, both INDEX-MATCH functions

sized up to the next largest pipe diameter. This selected pipe diameter was used for all subsequent sections.

3.4 Post – Diameter

In the post diameter tab, which can be seen below in Figure 8, several other calculations which used the diameter were found.

Initial Values		**Velocity (m/s)**	1.507986872		
Diameter (m)	0.0254	Cross Sectional Area (m^2)	0.000506707		
Flow Rate (m^3/s)	0.000764108				
Dynamic Viscosity (N*s/m^	0.001307	**Reynolds Number (-)**	29297.15048		
Density (kg/m^3)	999.7	Density (kg/m^3)	999.7		
Vapor Pressure (Pa)	1228	Diameter (m)	0.0254		
Roughness (m)	4.57317E-05	Dynamic Viscosity (N*s/m^2)	0.001307		
		Water Depth Above Siphon Entrance (h0) (m)			
		Diameter (m)	0.0254		
		Between Diameters		Water Depth (m	Min Depth (m)
			0.1	0.0508	0.3
			0.3	0.0254	0.7
			0.8	0.04318	2
		Chosen Depth (m)		0.3	
		Darcy Friction Factor (-)		0.027782674	
		Equivalent Roughness (m)		0.001800461	$\frac{1}{\sqrt{f}} = -2log_{10}\left(\frac{\varepsilon}{3.7D_h} + \frac{2.51}{Re\sqrt{f}}\right)$
		Reynolds Number (-)		29297.15048	

Figure 8: Post-Diameter Tab

Initial values were imported into this tab from previous sections for ease of calculations, which included the newly selected diameter, flow rate of the pipe, viscosity, density, vapor pressure, and the roughness of the pipe. From these values, the velocity was found by dividing the flow rate by the pipe's cross sectional area. The Reynolds number for pipe flow was found by its respective equation using the previously calculated velocity and diameter, as well as the other water properties. The Darcy friction factor was iteratively found through the use of the Colebrook equation, equivalent roughness of the pipe, and the Reynolds number.

In this section, the necessary water depth above the entrance to the siphon was also found, which is a recommendation from the Food and Agriculture Organization of the United

Nations for siphon design to prevent entrenchment of air into the pipe through the siphon entrance, and is based on the diameter of the pipe (Kovari, 1984). If the diameter was between 0.1 and 0.3 meters [3.94 in and 11.81 in], the water depth should be at least twice the size of the pipe diameter, while at a minimum being 0.3 meters [11.81 in]. If the diameter was between 0.3 and 0.8 meters [11.81 in and 31.50 in], the water depth should be at least the size of the diameter, while at a minimum being 0.7 meters [27.56 in]. And if the diameter was greater than 0.8 meters [31.50 in], the water depth should be at least the size of the diameter multiplied by 1.7, while at a minimum being 2 meters [78.74 in].

3.5 Pressure

Within the pressure tab, which can be seen below in Figure 9, the pressure at the locations within the siphon at risk of cavitating were found.

Initial Values			**Upstream Pressure Head (m)**	8.772801		**Vapor Pressure Head (m)**	1.125216
Density (kg/m^3)	999.7		Atmospheric Pressure Head (m)	9.301382		**Upstream Head (m)**	0.02413
Diameter (m)	0.0254		Top Water Level (m)	0.35052		Top Water Level (m)	0.35052
Velocity Head (m)	0.115903		Top of Pipe Level (m)	0.37465		Top of Pipe Level (m)	0.37465
Vapor Pressure (Pa)	1228		Velocity Head (m)	0.115903		**Downstream Head (m)**	0.25908
Absolute Pressure (Pa)	101354.7		Suction Head Minor Losses (m)	0.127494		Top Water Level (m)	0.35052
Top Water Level (m)	0.35052		Suction Head Major Losses (m)	0.261054		Bottom Water Level (m)	0.09144
Top of Pipe Level (m)	0.37465						
Bottom Water Depth (m)	0.09144		**Downstream Pressure Head (m)**	9.114217		**Maximum Lift of Siphon (m)**	8.705202
Friction Factor (-)	0.027783		Atmospheric Pressure Head (m)	9.301382		Atmospheric Pressure Head (m)	10.33487
Upstream Lengths (m)	2.059178		Top Water Level (m)	0.35052		Vapor Pressure Head (m)	1.125216
Downstream Lengths (m)	0.502969		Discharge Height (m)	0.09144		Velocity Head (m)	0.115903
Upstream Minor Loss Coef (-)	1.1		Velocity Head (m)	0.115903		Upstream Minor Losses (m)	0.127494
Total Minor Loss Coef (-)	2.3		Downstream Head Minor Losses (r	0.266578		Upstream Major Losses (m)	0.261054
			Downstream Head Major Losses (r	0.063764			

Figure 9: Pressure Tab

As was seen in previous tabs, several initial values were brought into this tab for ease of calculations of the various pressure values. The upstream pressure head was found based on equation 9, originally introduced in section 2. This is the first critical point in the siphon where the lowest pressure would occur, and is seen as point D in Figure 2. Equation 9 was reconstructed in head form, and can be seen below as equation 11.

$$\frac{P_D}{\rho g} = \frac{P_A}{\rho g} + h_A - h_D - \frac{v_D^2}{2g} - h_L \quad (11)$$

Points D and A are the positions of the pressure concern near the crest of the siphon and atmospheric pressure respectively, and can be further seen in Figure 2. Similarly, the downstream pressure head was found based on equation 10, also introduced in section 2. This is the second critical point in the siphon where pressure concerns may be found, and it occurs prior to the siphon entering the lower reservoir, and is where the highest amount of friction would occur within the piping. This location can be seen as point F in Figure 2. This equation was reconstructed in head form as well, and can be seen below, as equation 12.

$$\frac{P_F}{\rho g} = \frac{P_A}{\rho g} + h_A - h_F - \frac{v_F^2}{2g} - h_L \quad (12)$$

Points F and A are the positions of pressure concern prior to entering the lower reservoir and the atmospheric pressure location respectively, and can be further seen in Figure 2. The atmospheric pressure for the location for both upstream and downstream pressure heads were multiplied by 0.9 to incorporate a safety factor, in accordance with guidelines set by the Food and Agriculture Organization of the United Nations (Kovari, 1984). As well the vapor pressure of the water was converted to head form, and will be used later on in the siphon design tool to better understand the risk of cavitation. One meter of head was added to the vapor pressure as a safety factor, in accordance with guidelines by the Food and Agriculture Organization of the United Nations, to find the allowable pressure head (Kovari, 1984). The overall upstream head of the siphon was also found, which is the difference between the depth of the upper reservoir and the top of the pipe. As well, the overall head was found, which is the difference between the upper and lower reservoirs.

The maximum lift of the siphon was also found, at the request of Rickly Hydropower. This is a theoretical point where vapor pressure would occur if siphonic action were able to lift to this point, and can be seen further detailed below in equation 13.

$$h_{max} = \frac{P_A}{\rho g} - \frac{P_{Vap}}{\rho g} - \frac{v^2}{2g} - h_L \quad (13)$$

Point A is the atmospheric pressure location, as was seen in Figure 2. h_{max} is the maximum lift of the siphon, and P_{Vap} is the vapor pressure of the liquid. In this calculation, safety factors were not included as it is a theoretical point.

3.6 Volume Flow

Within the volume flow tab, which can be seen below in Figure 10, several aspects corresponding to the flow of the siphon were calculated.

Pre Chosen Values			**Pressure to Prime Siphon (Pa)**	-30094.8
Atmospheric Pressure (Pa)	101625.6		Atmospheric Pressure Head (m)	9.340259
Density (kg/m^3)	998.2		Top Water Level (m)	7.0104
Diameter (m)	0.6096		Top of Pipe Level (m)	8.5344
Top Water Level (m)	7.0104		Priming Velocity Head (m)	0.232021
Top of Pipe Level (m)	8.5344		Upstream Minor Losses (m)	0.024246
Priming Velocity (m/s)	2.1336		Upstream Major Losses (m)	0.255223
Friction Factor (-)	0.012063			
Upstream Lengths (m)	5.28066		**Froude Number (-)**	2.238375
Upstream Loss Coef (-)	1.1		Hydraulic Diameter	0.478779
Velocity (m/s)	4.851038		Cross Sectional Area	0.291864
Flow Rate (m^3/s)	1.415841		Top of Water Width	0.6096
Upper Reservoir Depth	7.0104			
Lower Reservoir Depth	1.524		**Square Footage of Intake (m^2)**	3.096765
			Necessary Velocity (m/s)	0.4572
			Maximum Possible Flow Rate(m^	3.02812
			Max Velocity (m/s)	10.37512
			Cross Sectional Area (m^2)	0.291864

Figure 10: Volume Flow Tab

Similar to the other tabs, several initial values were brought into this one for ease of calculations. First, the initial pressure below atmospheric necessary for the priming of the siphon

was calculated. This initial pressure was found through a variation of the head form of Bernoulli's principle, seen below as equation 14.

$$\frac{P_{Priming}}{\rho g} = \frac{P_A}{\rho g} + h_A - h_D - \frac{v_{priming}^2}{2g} - h_L \quad (14)$$

Where $P_{Priming}$ and $v_{Priming}$ are the priming pressures and velocities, respectively. Points D and A are the positions of pressure near the crest of the siphon – where the lowest pressure would occur in the siphon – and the location of atmospheric pressure at the upper reservoir respectively, and can be further seen in Figure 2. The atmospheric pressure within this equation was multiplied by a factor of safety of 0.9 in accordance with guidelines recommended by the Food and Agriculture Organization of the United Nations (Kovari, 1984). The priming velocity is based on recommendations by the URS Corporation (URS Corporation, 2010), who had recommended a priming velocity of 2.133 m/s [7 ft/s] in order to flush all air out of the pipe so it can flow full. The atmospheric pressure was subtracted from this value, in order to find the gauge pressure necessary to begin siphonic activity.

Note that the Froude number is shown here too. The Froude number is relevant for open channel flow, relating the flow velocity to wave speed. It can be seen below, in equation 15.

$$Fr = \frac{v}{\sqrt{gD_h}} \quad (15)$$

Where v is the velocity of the fluid, g is gravitational acceleration, and D_h is the hydraulic depth of the fluid. The hydraulic diameter is defined as the cross sectional area of the fluid divided by the top width of the fluid. Due to the effects viscosity has on siphonic flow, water can flow at times at the top of the siphon with air still in the system, which would be considered open channel flow. It is thought the performance of the siphon may be predicted in some way based on this number. This being said, no supporting literature was found on this aspect of siphon flow

and thus was not pursued any further. Within this generator this value was calculated assuming the pipe flowed at half full, and the cross sectional area and fluid width were found accordingly.

The square footage of the intake to achieve minimal approach velocity was also found for fish protection. This square footage is based on the concept that fish can sense fluid velocity moving at 0.4572 m/s [1.5 ft/s] and swim out of harm's way of the siphon, and was recommended based on Rickly's internal tools. There is some contention to this value being 0.4572 m/s [1.5 ft/s], as other sources describe it more closely to 0.1524 m/s [0.5 ft/s] (Coutant, Bevelheimer, & Cada, 1999). If this value was to be changed, the Necessary Value cell within the volume flow tab would need to be modified. The total volume flow rate of the siphon system is divided by this value to obtain the ideal square footage of the intake.

As well, the maximum volume flow rate capable of being produced by this siphon hydro system was also found. This was the calculated as the maximum velocity based on the head of the site, multiplied by the cross sectional area of the piping. This value is used to compare the input flow rate to, and understand whether the flow rate input by the user is theoretically capable of being produced by the siphon.

3.7 Output

Finally, the output tab of the Excel siphon design tool was created to display the results to the user in an easily understood fashion. The output tab can be seen below, in Figure 11.

Rickly
Harnessing the World's Water

Output	
SIPHON SIZING	
Siphon Diameter (in)	1
Total Length (ft)	9
Depth of intake (ft)	1
PRESSURE CONCERNS	
Siphon Max Lift (ft)	28.560375
Upstream Pressure Head (ft)	28.7821566
Downstream Pressure Head (ft)	29.9022864
Vapor Pressure Head (ft)	3.69165339
Upstream Head (ft)	0.07916667
Downstream Head (ft)	0.85
Upstream Cavitation?	NO
Downstream Cavitation?	NO
VOLUME FLOW	
Priming Pressure (psi)	-2.93
Froude Number	3.02096851
Square Footage To Achieve Min Approach Velocity (ft^2)	0.01798947
Maximum Possible Flow Rate	0.04034403
Achieve Input Flow Rate?	YES

Figure 11: Output Tab

Initially the sizing parameters of the siphon were presented, which included the selected diameter of the siphon, the total length of the system, and the necessary depth of the intake. Next, a variety of pressure concerns were displayed, including the maximum lift of the siphon, the upstream and downstream pressure heads, the vapor pressure head of the system, and the overall upstream and downstream heads of the siphon itself. The upstream pressure head was compared to the vapor pressure and to the upstream head, to make sure that it would both not cavitate and was able to get over the crest of the dam itself. The downstream pressure head was compared to the vapor pressure head and the overall head of the site, as if this downstream pressure head was lower than the overall head, the pipe would cavitate. Finally, the volume flow elements calculated in the previous tab were displayed in its according section, and the maximum possible flow rate capable of being produced by the siphon was found.

Chapter 4: Flume Characterization

Throughout this section, the flume used throughout the validation of the above siphon design tool is discussed. First the flume is described and the use of it is discussed. Next, flow rate measurements were found in a manner of ways and compared to the flow rates presented in the flume manual, as there was concern of the accuracy of flow rates presented in the manual.

4.1 Flume Description

Within this experiment, an Engineering Laboratory Design teaching flume provided by the Department of Civil, Environmental, and Geodetic Engineering was used. The flume can be further seen below, in Figure 12. The flume has a height of 0.4572 m [18 in], width of 0.3048 m [12 in], and a length of 5.06 m [16.6 ft], with plexiglass walls and floor.

Figure 12: Ohio State Teaching Flume

The flume works by recirculating water from a large reservoir located at the end of the body through the open channel of the flume itself. The flume can be operated over a variety of flow rates, using two separate pumps, and can be varied between 0.000293 m^3/s [0.01033 cfs] and 0.016823 m^3/s [0.59409 cfs], according to the provided manual. These flow rates are

specified and controlled through a user interface by a variety of pump frequency rates, ranging from 0 Hz to 60 Hz. The manual provides a table and a graphic relating each pump rate to a specific flow rate, the graphic of which can be seen below in Figure 13.

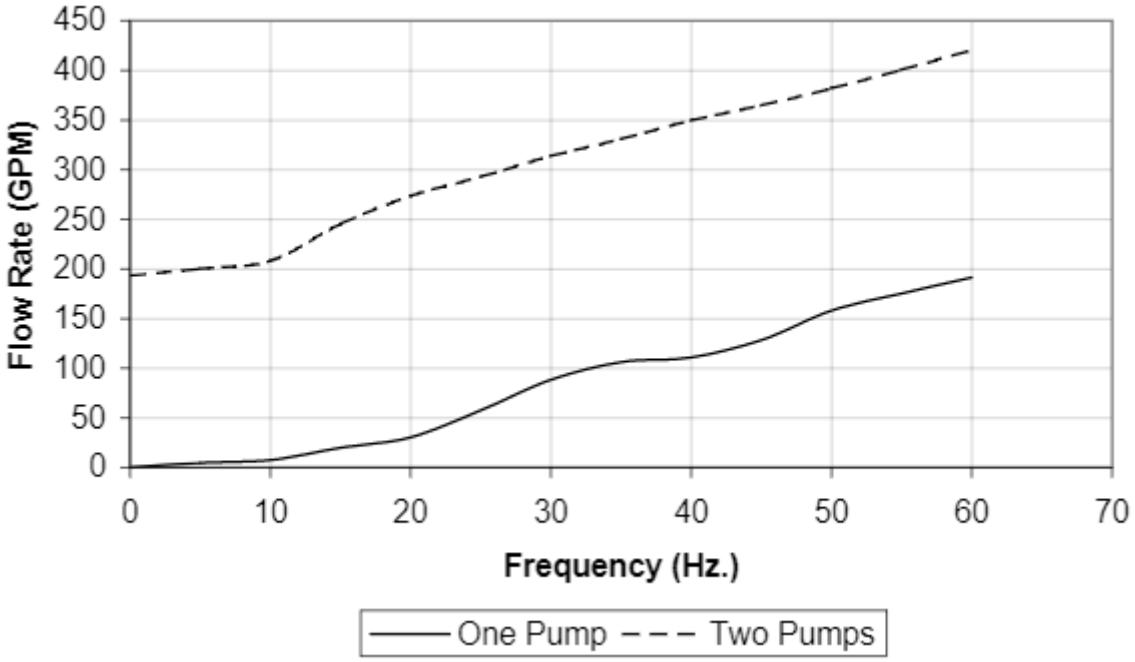

Figure 13: Pump Frequency vs Flow Rate at 0° Slope

As is seen above, one of the pumps can be varied between 0 and 60 Hz to change the overall flow rate, while the second can only be run on either totally off (0 Hz) or totally on (60 Hz). By varying the frequency within these two pumps, the maximum possible flow rate of 0.016823 m^3/s [0.59409 cfs] can be reached. The user may also control the depth of water throughout the body by raising a tailgate to a desired height, as well as the angle the water flows at, through a tilt setting. Throughout all experimentation performed within this flume, the tilt was set to 0°. These variations are also controlled using the user interface, an image of which can be seen below, in Figure 14.

Figure 14: Flume Operating Panel

Finally, different obstructions to the flow, such as weirs, can be placed within the flume through a series of 4.76 mm [3/16 in] tapped holes along the base of the flume, which were placed 7.62 cm [3 in] apart from one another horizontally, and 15.24 cm [6 in] apart along the flume basin. A further image of the mounting screws can be seen below, in Figure 15.

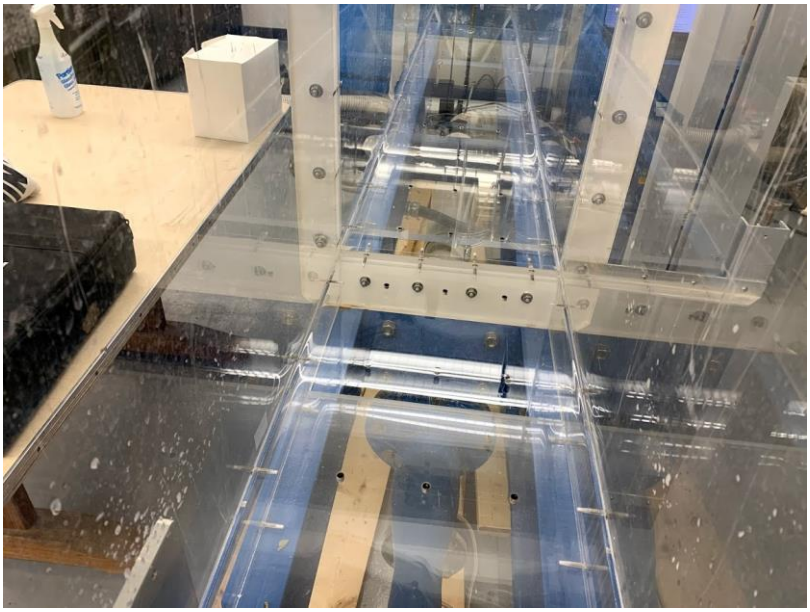

Figure 15: Flume Mounting Screws

4.2 Flow Rate Measurements

There was a concern of the accuracy of the flow rate values presented in the flume manual as the pumps controlling the flow rate were dated, among other concerns. The flow rates within the manual were presented as pump rates in Hz, values which could be converted to cubic feet per second and gallons per minute. To further analyze this, the flow rates within the flume were measured using three different devices – a pitot static tube, a venturi meter, and a sharp crested v-shaped weir – and their values were compared amongst themselves, as well as against the values reported in the flume manual.

4.2.1 Pitot Static Tube Measurements

A pitot static tube is a device often used to take flow measurements, specifically involving fluid velocity at a point, and has been studied and employed extensively in fluid dynamic measurements. This device works by measuring pressure values at two separate

locations in the flow – which through the use of Bernoulli's equation can be employed to find the fluid velocity. These locations can be seen below as locations 1 and 2, in Figure 16.

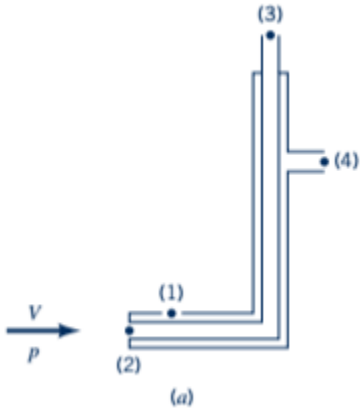

Figure 16: Pitot Static Tube Cross Section (Gerhart, Gerhart, & Hochstein, 2016, p. 115)

The stagnation pressure is the pressure of the fluid when it comes to a complete halt at the entrance of the pitot tube. It is measured through the front facing hole (or location 2 in this diagram) and consists of both a static and dynamic pressure component, since the dynamic pressure has been converted to static at the stagnation point. The static pressure of the flow is measured from location 1 in the diagram, and is the actual thermodynamic pressure of the fluid as it moves past the device (Gerhart, Gerhart, & Hochstein, 2016, pp. 113-117). Bernoulli's equation describes the sum of the stagnation and hydrostatic pressure terms along a streamline, however, as a horizontal pitot static tube measures flow at the same elevation, the hydrostatic pressure is assumed to be zero. To find the dynamic pressure of the fluid, from which velocity can be calculated, one must subtract the static pressure from the stagnation pressure. This can be further seen through equations 16 and 17 below.

$$P_{Stagnation} = P_{Static} + P_{Dynamic} = P_{Static} + \frac{1}{2}\rho v^2 \quad (16)$$

$$v^2 = \frac{2}{\rho}(P_{Stagnation} - P_{Static}) \quad (17)$$

With ρ being the fluid density, and v being the fluid velocity. In order to record the values for stagnation and static pressure, these must be measured by connecting a pressure gage to the two ports of the pitot tube. For the experimental setup described here, a traditional liquid manometer was employed. This device relates a water column height to the amount of pressure seen in a fluid. The pitot tube used for this analysis was acquired from Engineering Laboratory Design, the flume manufacturer. An image of the pitot tube and manometer used for the measurements can be seen below, in Figure 17.

Figure 17: Pitot Tube and Manometer

To obtain accurate flow measurements, the pitot tube was tested at 3 different pump frequency rates (40 Hz, 45 Hz, and 50 Hz) and at three different depths of flow within the flume

for each flow rate (9.144 cm [0.3 ft], 12.192 cm [0.4 ft], 15.240 cm [0.5 ft]). The flow depths were created by raising the tailgate to different levels, and measuring the subsequent depth of the fluid. Velocities at 5 different points within each flow and depth combination were then analyzed, which varied from the bottom of the flume itself and continued until the pitot tube was near the surface of the open channel flow. Each flow rate and depth combination was only tested once. As well, these velocities were analyzed at the center of the flume to best avoid any boundary layer effects from the side walls of the flume. As the water flows through the flume channel, a boundary layer will form at the flume bed due to the viscous interaction between the fluid and the glass wall. We hence expect to see a velocity profile captured when measuring the velocity at varying heights above the flume bed. An equation approximating flow velocity to the height within the boundary layer is given in equation 18.

$$\frac{V}{V_{Max}} = \left(\frac{y}{\delta}\right)^{\frac{1}{7}} \quad (18)$$

In this equation, V, the fluid velocity at a specific point in the boundary layer, is dependent on y, the vertical location above the wall where the flow was measured, δ, the total height of the boundary layer, and V_{Max}, the maximum velocity of the flow. This specific equation only is an approximation for turbulent Reynolds numbers, however, it was assumed that the flow throughout all measured flow rates was turbulent (Chanson, 2004, p. 27). Several sources describe this correlation to be appropriate (Cengel & Cimbala, 2006, p. 529; Chanson, 2004)

The velocity measurements for each flow rate and depth combination were plotted and compared to the calculated velocity from equation 18. Within this calculation, the maximum velocity was assumed to be the velocity point measurement nearest to the surface of the flow, the

total height of the boundary layer was assumed to be the water depth within the flume, and values for y distance above the base of flume were varied to produce a smooth plot of the flow velocity. This plot can be seen below, in Figure 18.

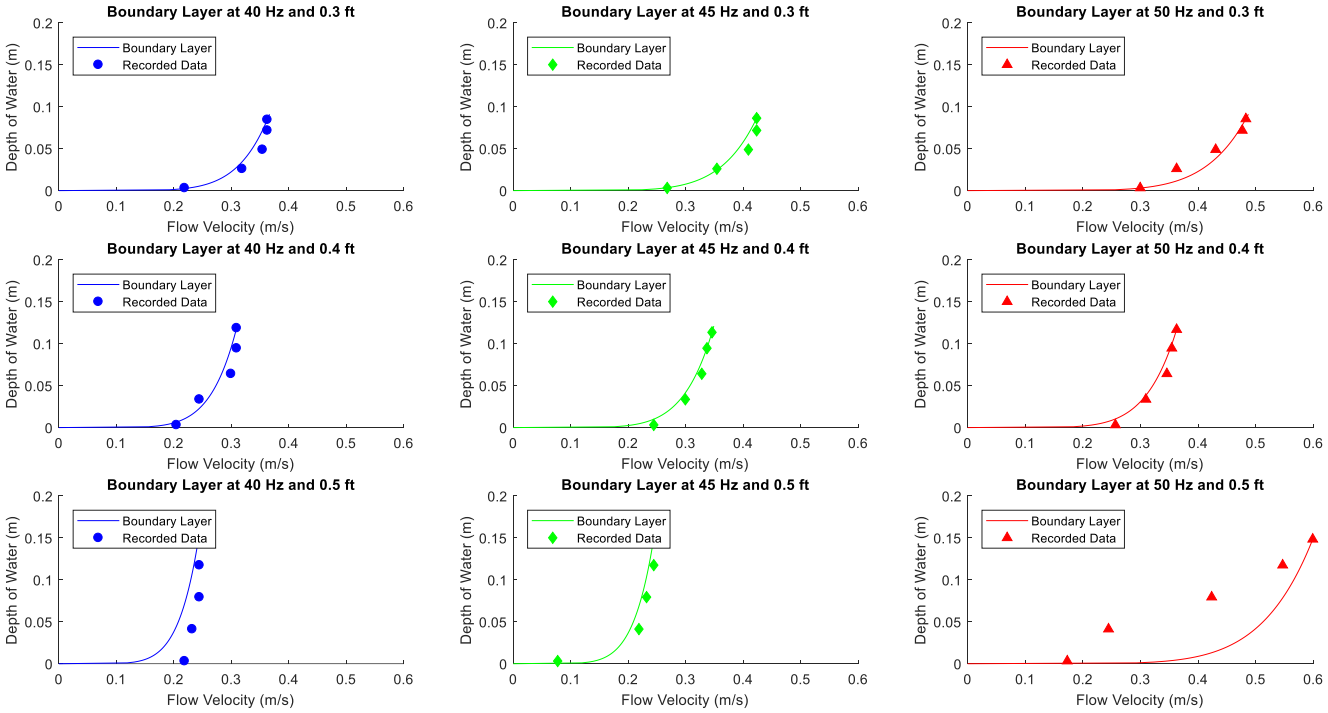

Figure 18: Point Velocity Measurements vs Theoretical Boundary Layer

The point velocity measurements compared reasonably well to the theoretical velocities calculated from equation 18. While there were some errors, this could be explained from the inaccuracy of measurements using a liquid manometer device.

An integration was subsequently performed using the measured flow velocity values with respect to the depth of the water the data value was recorded at. This integrated value was then divided by the total depth of the water to find an average velocity value, which was multiplied by the width of the flume, as well as the depth of the water, to find the overall flow rate for each

depth and flow combination. The equation used to calculate the flow rate can be seen below, as equation 19.

$$Q = AV = hwV \quad (19)$$

Where w is the width of the flume, h is the chosen depth of water for that specific measurement, Q is the flow rate, and V is the average velocity of the flow. The flow rates measured from each water depth were then averaged to find an average flow rate value. The results from the tests can be seen below, in Table 1, and are better visualized using a graph, seen below as Figure 19.

Table 1: Measured Flow Rate From Pitot Tube (m3/s)

Fluid Depth (m)	40 Hz	45 Hz	50 Hz
0.09144	0.00813	0.00961	0.0102
0.12192	0.00971	0.0105	0.0114
0.15240	0.0111	0.00951	0.0173
Average	0.00964	0.00987	0.0130

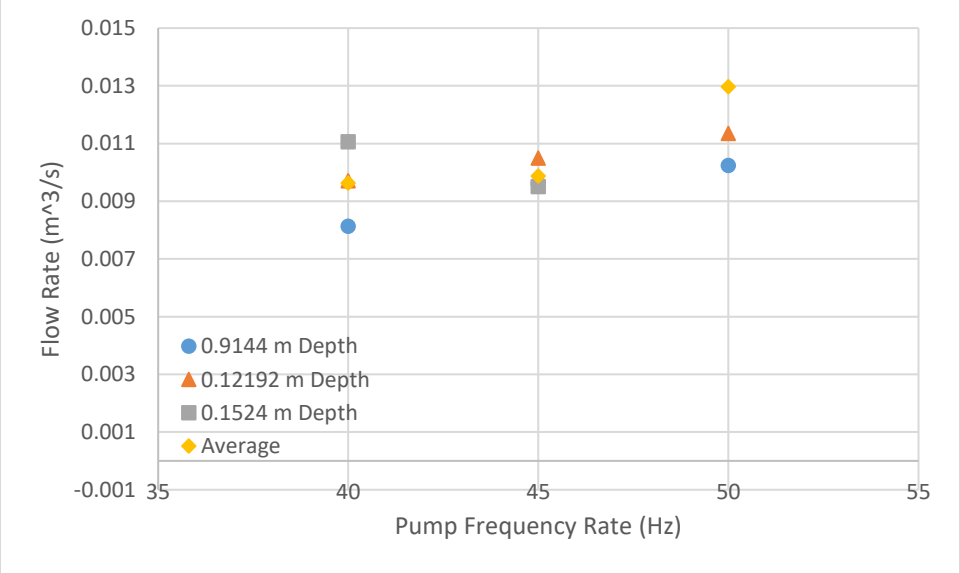

Figure 19: Flow Rate vs Pump Rate (Hz) Using a Pitot Static Tube

One would predict the flow rate to increase as the pump rate setting increased, however, the measured average flow rates did not change much, and some of the measurements did not

follow the expected trend – specifically when the water depth was 15.24 centimeter [0.5 ft], as the flow rate decreased between 40 Hz and 45 Hz, when it should have increased. Further, for a given pump frequency setting, the recorded flow rate should be roughly constant, as the only aspect that changes is the tailgate setting. The change in flow rates can be explained from inaccuracy in measurement, as the difference in water height found using the liquid manometer was difficult to accurately record.

4.2.2 Venturi Meter Measurements

A venturi meter is flow measuring device specifically designed for flow rates. The venturi meter works by using a combination of the continuity equation – or the statement that a flow rate will stay constant over a changing area – and Bernoulli's equation to calculate the flow rate. The equation for continuity can be seen below, as equation 20.

$$Q = A_1 V_1 = A_2 V_2 \quad (20)$$

Where points 1 and 2 are two different locations in the flow with varying cross sectional areas, such that $A_1 > A_2$. These two locations can be better visualized through a diagram, which is located below as Figure 20.

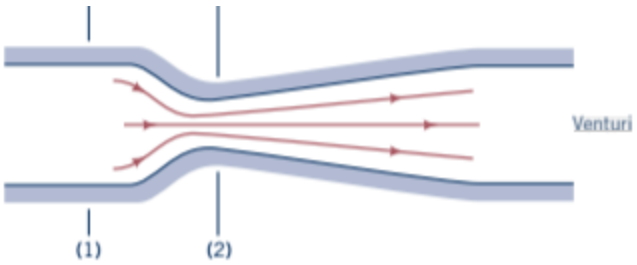

Figure 20: Venturi Meter Diagram (Gerhart, Gerhart, & Hochstein, 2016, p. 127)

In a venturi meter, the static pressure at locations 1 and 2 are measured. By combining the equation for continuity with Bernoulli's principle, the static pressure at locations 1 and 2, as

well as the assumption that the change in hydrostatic pressure is negligible, one may generate equation 21 below.

$$Q = A_2 \sqrt{\frac{2(P_1 - P_2)}{\rho(1 - \left(\frac{A_2}{A_1}\right)^2}} \quad (21)$$

The inner diameters of the piping at locations 1 and 2 were known constant values found in the flume manual, and were 0.10155 m [4 in] and 0.06096 m [2.4 in] respectively. The static pressures at locations 1 and 2 were found using a traditional manometer, similar to what was used for the pitot tube. A small amount of error may have been present in these measurements due to residue found on the inside of the tubes, however, this was assumed to be negligible. An image of the venturi meter used for the measurements can be seen below, in Figure 21.

Figure 21: Venturi Meter

The venturi meter is located directly beneath the open channel of the flume itself, and is directly in the path for the flow to go through prior to entering the open channel. To match the measurements of the pitot tube, the venturi meter pressure measurements were taken over the same flow rate (40 Hz, 45 Hz, and 50 Hz) and water depth (0.09144 m [0.3 ft], 0.12192 m [0.4 ft], 0.15240 m [0.5 ft]) combinations. While the depth of the water should not have theoretically

had an effect on the flow readings from the venturi meter, there was a fear that the hydrostatic pressure of the water depth may have had some effect on pump performance, which, in turn, would have resulted in a lower flow rate. The results from these tests can be seen below, in Table 2 and are better visualized as a graph, seen below as Figure 22.

Table 2: Measured Flow Rate Using Venturi Meter (m3/s)

Depth of Water (m)	40 Hz	45 Hz	50 Hz
0.09144	0.00900	0.0102	0.0113
0.12192	0.00895	0.0101	0.0113
0.1524	0.00890	0.0101	0.0112
Average	0.00895	0.0101	0.0113

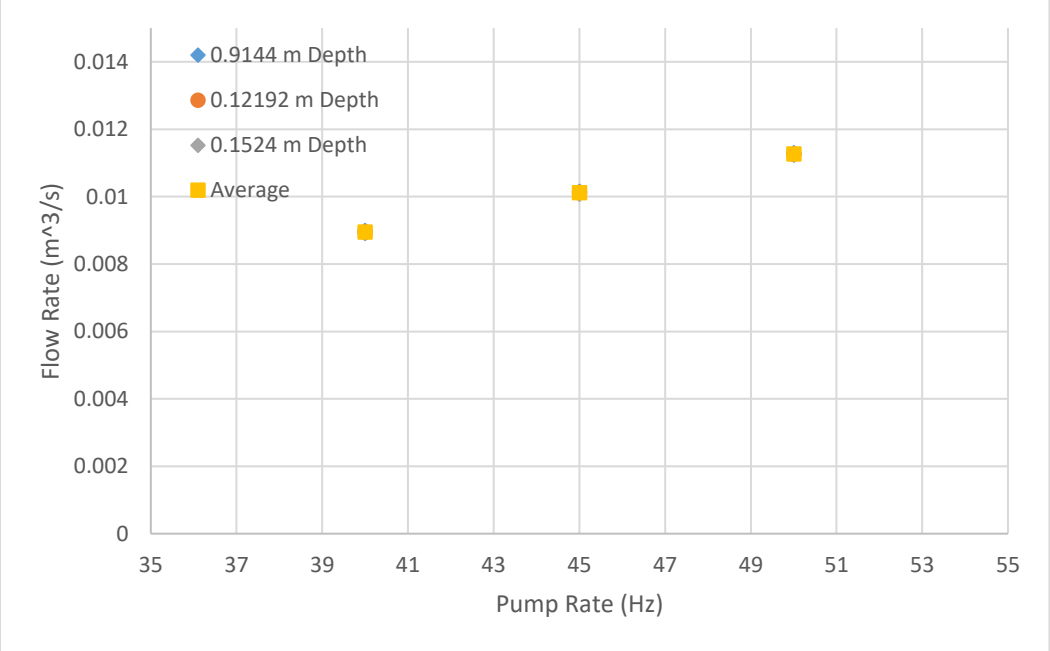

Figure 22: Measured Flow Rate vs Pump Rate for Venturi Meter

Similar to what was stated for the pitot tube measurements above, one would expect the flow rate to increase steadily when the pump rate was increased. The measured flow rate values for the venturi meter followed this trendline, increasing in a linear fashion. The flow rates for each measurement were so similar to one another that they were plotted over one another. In addition, the hydrostatic pressure from the water depth did not have an effect on the flow rate

measurements, as the difference in measured flow rate for each water depth was negligible. This seems to show that the hydrostatic pressure within the flume does not have an effect on the pump performance. However, the water depth was only varied by 3.048 cm [0.1 ft] between measurements, and so a wide range of data points was not analyzed for this experiment. Further testing over a larger range of water depths should be further explored.

4.2.3 Sharp Crested V-Notch Weir Measurements

In addition to the above two methods, the flow rate was measured using a sharp crested V-notched weir. In this method, the fluid is allowed to overtop the sharp crested weir in use, and the height of the fluid overtopping can be directly related to a specific flow rate. Similar to the methods for measuring flow using the pitot tube and the venturi meter, the flow measured from a sharp crested weir can be derived using Bernoulli's principle. In this equation, it is assumed that the velocity profile upstream is uniform, the pressure at the weir edge is atmospheric, and the fluid flows horizontally over the weir plate itself with a nonuniform velocity profile (Gerhart, Gerhart, & Hochstein, 2016, pp. 587-589). This can be better visualized below, in Figure 23.

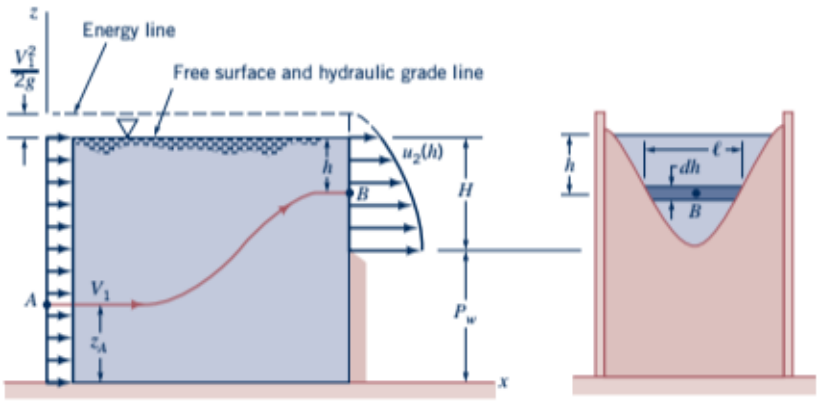

Figure 23: Sharp Crested Weir Diagram (Gerhart, Gerhart, & Hochstein, 2016)

Based on these assumptions, Bernoulli's principle can be re-written below as equation 22, where H is the total height above the weir crest, P_w is the weir height, z_a is the height of a fluid

particle upstream, h is the height of a fluid particle overtopping the weir, and u_2 is the velocity of the fluid overtopping the weir.

$$\frac{P_A}{\rho g} + \frac{V_1^2}{2g} + Z_a = (H + P_w - h) + \frac{u_2^2}{2g} \quad (22)$$

However, by assuming that the total head for any upstream particle is the same and would equate to the weir height added to the water height above the v-notch itself, equation 22 can be rewritten and solved for fluid velocity of the weir , which is seen as equation 23 below.

$$u_2 = \sqrt{2g\left(h + \frac{V_1^2}{2g}\right)} \quad (23)$$

By integrating this velocity over the fluid height above the sharp crested weir, multiplying by a length factor dependent on the weir plate geometry, and adding an experimentally determined correction factor (seen as C_{wt}) to account for the viscosity and surface tension affects, flow rate can be determined (Gerhart, Gerhart, & Hochstein, 2016, pp. 587-589). While flow rate may be determined for different weir plate geometries, a V-shape weir was used for these experiments as a measurement for the height above the weir edge can be determined most efficiently. This flow rate equation can be seen as equation 24 below.

$$Q = C_{wt}\frac{8}{15}\tan\left(\frac{\theta}{2}\right)\sqrt{2g}H^{5/2} \quad (24)$$

Where θ is the angle of the notch within the weir. As is seen, the flow rate over a sharp crest V-shaped weir is directly dependent on the angle of the notch within the weir itself, and the water depth measured from the base of the notch.

When determining the flow rates for using this measurement technique, the angle of the notch was found through measurements of the weir geometry using a tape measure and

trigonometric principles, and was found to be 90 degrees. The weir used for the flow rate measurements can be seen below, in Figure 24.

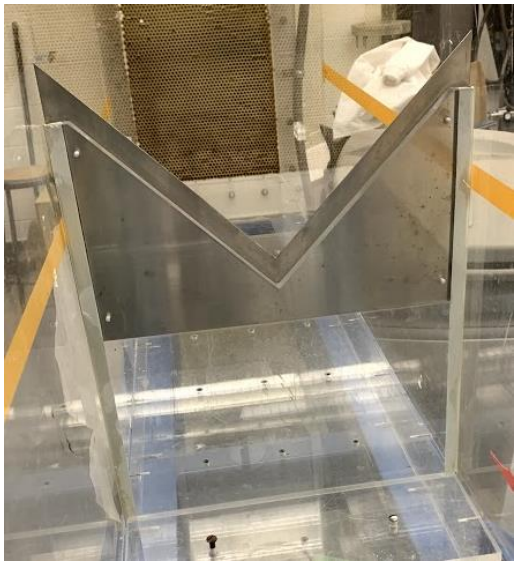

Figure 24: V-Shaped Weir

To match the measurements found using the pitot tube and venturi meter, flow rates were measured over 40 Hz, 45 Hz, and 50 Hz. The depth of water past the V-shaped weir was not changed and the tailgate was left completely open for this measurement as the weir was positioned in the open channel of the flume itself. The height of the fluid above the notch base was measured using a tape measure as the flow was overtopping the sharp crested weir. Due to the inaccuracy in measurement technique using a tape measure to find the height, an inherent error is expected in the values. Flow measurements from these tests can be seen below in Table 3, and are better visualized as a graph, seen below as Figure 25. As is expected, the flow rate increases linearly as the pump rate is also increased.

Table 3: Measured Flow Rate Using Sharp Crested V-Shape Weir (m3/s)

Pump Rate (Hz)	40 Hz	45 Hz	50 Hz
Flow Rate (m^3/s)	0.00795	0.00871	0.00898

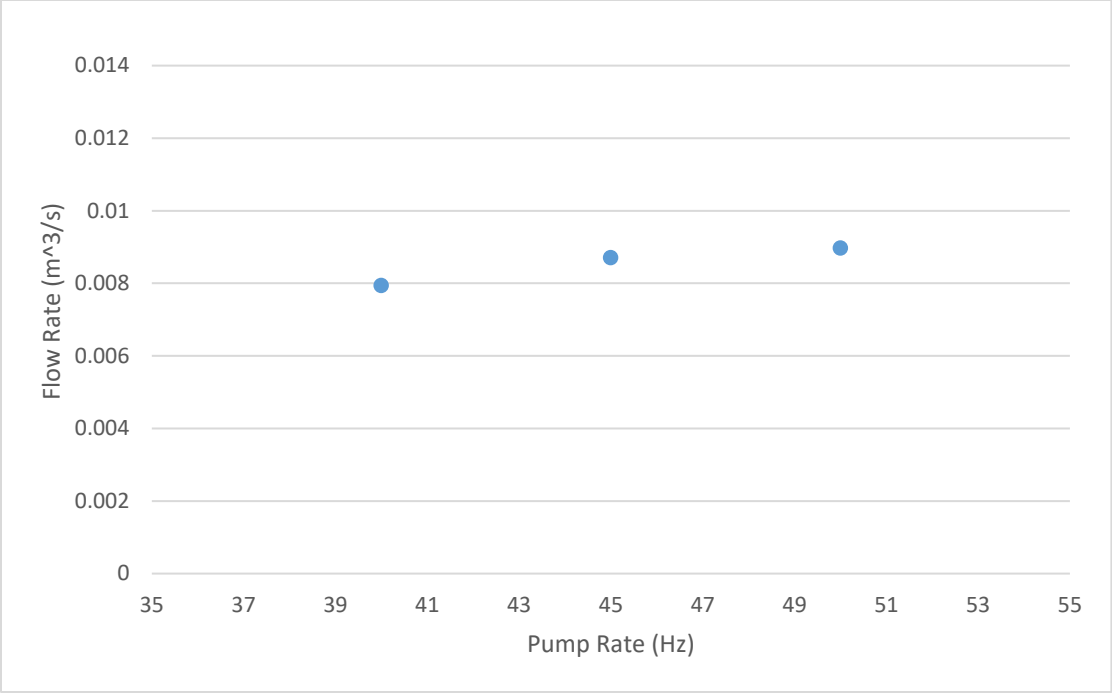

Figure 25: Measured Flow Rate vs Pump Rate for V-Shaped Weir

4.2.4 Comparison of Results

The average values for each flow rate measuring method along with the values presented in the flume manual were tabulated and can be seen below in Table 4. The differences between each flow rate can be better visualized in a graph, seen below as Figure 26.

Table 4: Average Flow Rates for All Measurement Techniques

Pump Rate (Hz)	Flume Manual Q (m^3/s)	Pitot Tube Q (m^3/s)	Venturi Meter Q (m^3/s)	Sharp Crested Weir Q (m^3/s)
40 Hz	0.00700	0.00964	0.00895	0.00795
45 Hz	0.00810	0.00987	0.0101	0.00871
50 Hz	0.00998	0.0130	0.0113	0.00898

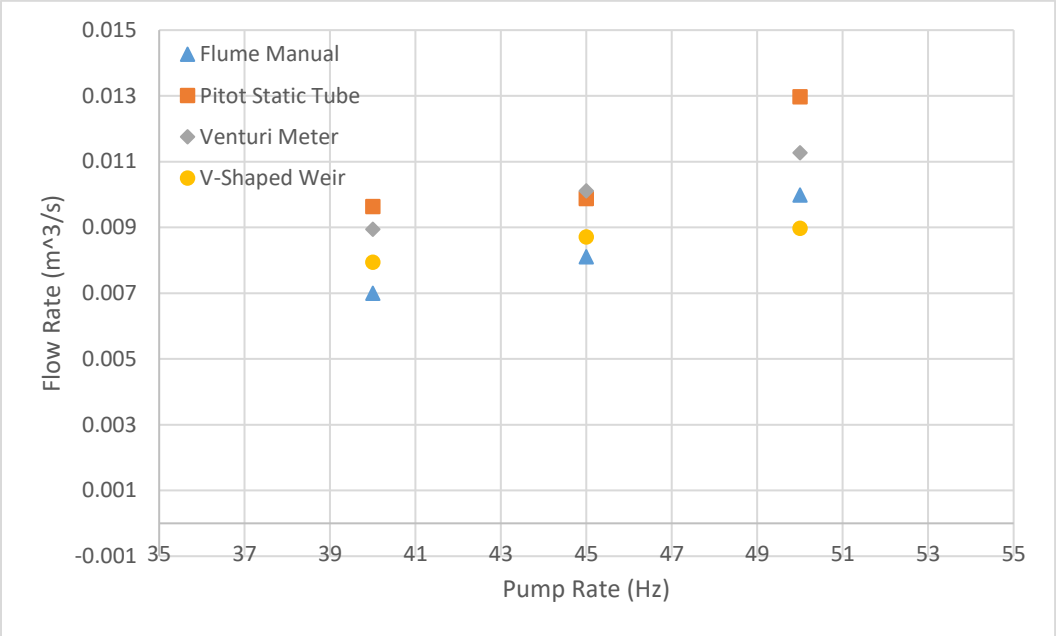

Figure 26: Flow Measurements

The flow measurements for the pitot tube were found to be, on average, larger than the ones found using the venturi meter and the weir. The measurements found by the venturi meter were between those found using the pitot tube and sharp crested weir. At a pump rate of 45 Hz, the data found between the pitot static tube and venturi meter matched well. This being said, there was more variance of the flow rate results when measured at other pump rates. The measurements described by the sharp-crested weir were found to be significantly lower than those measured by the pitot tube and venturi meter. Due to error in measurement techniques using the V-shaped weir, it is safe to say that the results found from the V-shaped weir consistently underpredicted the flow rate. Even with the error in measurements from the techniques, the flow rates for all 3 techniques were significantly higher than the flow rates reported in the flume manual – on average, 30% greater for the pitot tube values, 22% greater for the venturi meter values, and 3.7% greater for the sharp crested weir values. Based on these observations, it can be stated that the flow measurements found in the flume manual are

erroneous and greatly underestimate the actual flow found in the open channel of the flume. This may be due to the chart having been created using flow measurements with the tailgate raised significantly, as a high hydrostatic pressure within the flume may have had an effect on pump performance. As the flow measurements found using the venturi meter contained the least amount of observable error, best matched what was expected of the flow values, and were the most efficient to obtain for the testing of the siphon system, this measurement tool was used for the remainder of the experimentation.

Chapter 5: Experimental Siphon Tool Validation

Throughout the following section, the validation of the excel design tool described in section 3 will be explored through the creation of a scale model dam and siphon system. First, the design of the dam and siphon used in the validation is discussed. Next, the digital manometer used to take pressure measurements of the siphon system's accuracy was verified. Finally, pressure measurements were taken from pressure taps along the constructed siphon itself and compared to the expected values at the two critical pressure locations described by the design tool for validation.

5.1 Dam and Siphon Design

A dam and siphon system was constructed to most closely model a real system produced by Rickly Hydropower. Dam characteristics from a site owned by Rickly – including the dam dimensions, top and bottom water depths, and water temperature and pressure – were scaled down so as to fit in the teaching flume. These dimensions were scaled based on the dam height, as a maximum height within the flume of 14 inches was deemed appropriate to avoid flooding in case the dam overtopped. The ratio between the height of the full scale dam and this flume maximum height was used to scale all other dimensions.

These dimensions were then slightly modified to best make use of available materials. The angle on the inside of the dam (between the dam base and the down leg of the siphon) was reduced from 74° to 60° so as to make use of a 60° pipe fitting, as 74° pipe fittings are not commonly produced As well, the width of the top of the dam was increased from 1 inch to 3 inches to incorporate a clearance for pipe fittings. The final dimensions for the dam can be seen below, in Figure 27.

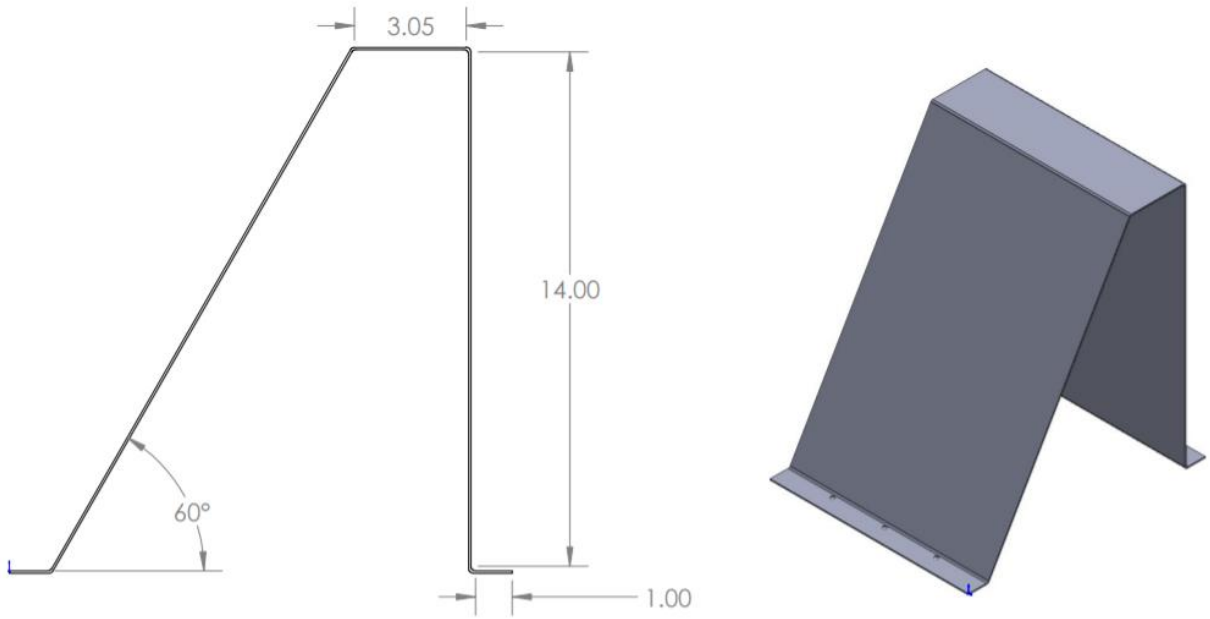

Figure 27: Dam Cross Section

A sheet of 28.575 cm x 121.92 cm x 0.15875 cm [11.25” x 48” x 1/16”] 3003 Aluminum was purchased to fabricate the dam itself. 3003 Aluminum was selected as it could bend well in a sheet metal brake. The size of 28.575 cm [11.25”] was selected to fit into the flume itself with some clearance. The sheet of aluminum was cut to size and bent at the necessary locations to obtain the listed dimensions above. Two small tabs, 2.54 cm [1”] wide, were added to the front and back of the dam with three 0.635 cm [1/4”] holes drilled, so as to mount the dam to the tapped holes within the base of flume channel. As well, three acrylic 0.635 cm [1/4”] thick panels, with dimensions equivalent to the inner dimensions of the sheet metal dam, were purchased and mounted on the inside of the dam so as to provide further structural rigidity. An image of the complete dam itself can be seen below, in Figure 28.

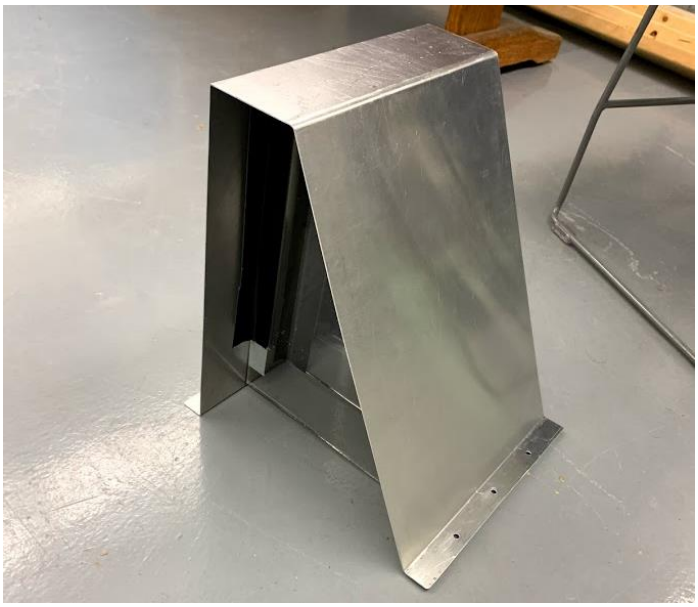

Figure 28: Sheet Metal Dam

The dimensions from this dam were then placed into the Excel siphon design tool – along with an initial estimation of the flow rate through the siphon based on the head difference between the upper and lower reservoirs – to obtain an estimation of the necessary diameter for the piping to construct the siphon. A diameter of 5.08 cm [2 in] was selected based on the siphon design tool, and a 5.08 cm [2”] clear PVC pipe was purchased. Clear PVC was chosen to better visualize the flow of water through the siphon. In addition to the piping, a 5.08 cm [2”] 90° and a 5.08 cm [2”] 60° pipe fitting were purchased to construct the siphon over the dam itself. A 5.08 cm [2”] slip to female NPT fitting was also purchased to close the end of the siphon in order to prime the siphonic activity, as well as allow for variable flow rates through the creation of perforated caps.

The clear PVC was cut to size appropriately based on the dimensions of the dam, and the piping was glued to the PVC fittings using PVC cement. Pressure taps were drilled into the down leg of the siphon at the two locations where pressure was capable of dropping below the allowed vapor pressure – one near the crest of the siphon, and one near the base of the down leg. Clamp

on saddle taps were used so the fittings would not create an obstruction in the flow, as this would add further friction unaccounted for into the siphon, break the boundary layer formed within the piping, and better represent a full scale siphon hydro system. Due to constraints set by the dimensions of the PVC pipe and fittings, the pressure taps were located 11.43 cm [4.5 in] from crest of the siphon, and 8.89 cm [3.5 in] from the exit of the siphon. Because of this, the pressure obtained from these two locations would differ slightly from the true concerning low pressure regions. An image of the siphon created can be seen below, in Figure 29.

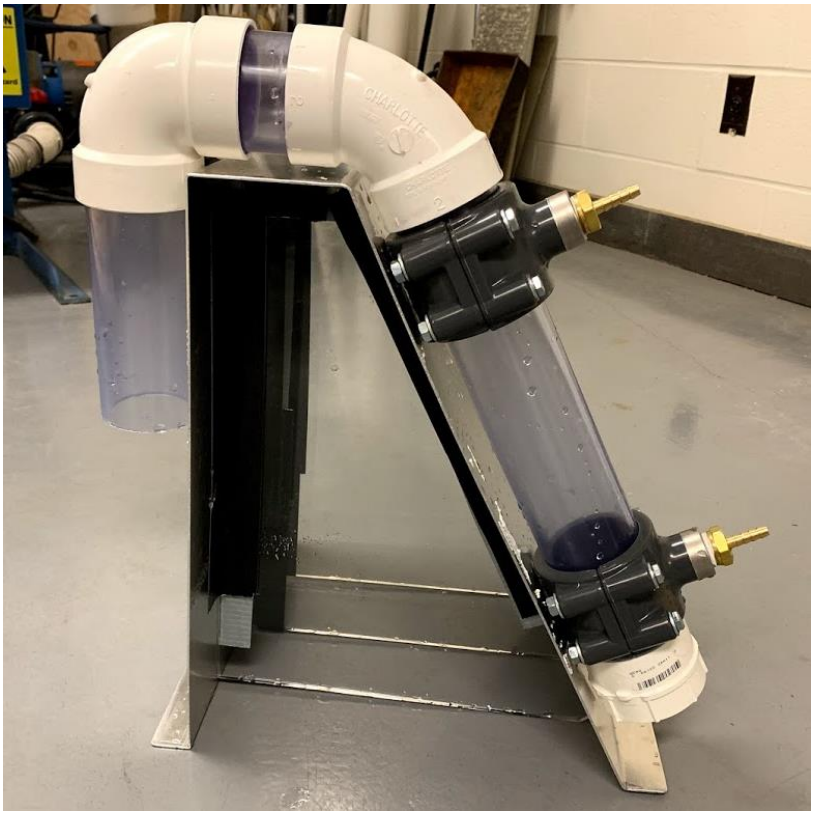

Figure 29: Constructed Siphon

To better validate the constructed siphon and dam system, the system was tested using a variety of flow rates. To best simulate this, two perforated caps were created in addition to the uncapped siphon, so as to slow the flow through the creation of an obstruction and an increase in the minor friction losses. This would allow tests to be performed at three different flow rates.

One where the end of the siphon was not capped and the fluid could flow freely, which would cause the greatest flow rate. One where the end of the siphon was capped with a coarsely perforated cap, which contained 20 6.35 mm [1/4 in] holes drilled through it, and allow for a medium flow rate. Finally, one where the end of the siphon was capped with a finely perforated cap, which contained 10 6.35 mm [1/4 in] holes drilled through it, and would allow for a slower flow rate.

As well, the number of holes within a perforated cap has a direct correlation to the pressure drop. As the number holes increase, the pressure drop behind the perforated cap would theoretically decrease (Malavasi, Messa, Fratino, & Pagano, 2012). Thereby, one would expect the uncapped flow to have the lowest pressure, the coarsely capped flow would have a medium pressure compared to the other two flows, and the finely capped flow to have the highest pressure throughout the siphon.

5.2 Venturi Pressure Results

To most accurately measure pressure results from the siphon system, a Dwyer 477 AV digital manometer was used to take the pressure readings within the siphon. As the pressure at the two locations within the flow would be below atmospheric, a digital manometer was deemed the most accurate device to use for these experiments. This digital manometer uses a piezoelectric sensor to take the air pressure measurements, and can measure positive pressure, negative pressure, or a pressure differential between ports (Dwyer Instruments, 2015). The instrument used can be seen below, in Figure 30.

Figure 30: Dwyer 477AV Digital Manometer (Dwyer Instruments, 2015)

However, there was a concern that the digital manometer on hand was reading inaccurate pressure values. To test this, the digital manometer was used to take readings of the pressure within the venturi meter, and compared to values found using the traditional manometer. Fittings were attached to the top of the traditional manometer, and the positive and negative pressure ports were fixed to the appropriate locations on these fittings correlating to the higher and lower static pressure locations produced by the venturi meter. An image of these connections can be seen below, in Figure 31.

Figure 31: Venturi Pressure Connections

For each test, the fittings were first vented to the atmosphere and the digital manometer was calibrated at this pressure. Next, the fittings were closed to the atmosphere. The pumps within the flume were turned on, and the pressure differential displayed on the digital manometer was continuously observed. It was apparent that there was a leak in one of the fittings as the pressure differential displayed would increase as the system reached steady state, reach a maximum value, at which point the pressure would suddenly begin decreasing again. In addition, if observed long enough, this value eventually reached and stayed at zero. To account for this, the maximum pressure differential displayed was used for the flow rate calculations. The flow rate values were subsequently calculated based on the flow rate equation for use with a venturi meter, seen as equation 21 in section 4, and compared to values found from the traditional manometer for pump rates of 35 Hz, 40 Hz, 45 Hz, and 50 Hz. A table comparing the flow rate values obtained using both traditional and digital manometers can be seen below, as Table 5.

Table 5: Flow Rate Measurements From Both Traditional and Digital Manometer

	Flow Rate (m^3/s)		
Pump Rate (Hz)	Traditional Manometer	Digital Manometer	Percent Difference
35	0.00805	0.00730	9.36%
40	0.00909	0.00842	7.42%
45	0.0102	0.00986	3.74%
50	0.0114	0.0105	8.15%

As is seen, the flow rate values obtained using both techniques compared well, and had a small percent difference for each measured flow rate. This difference in flow rate measurements can be at least partially accounted for from the known leak within the fitting used at the top of the manometer. Based on these results, the digital manometer was deemed accurate to use in measuring the pressure within the siphon.

5.3 Pressure Results from Siphon System

In the following section, pressure results obtained from the experimental siphonic system are discussed. First, the experimental setup is described, as well as how pressure measurements were specifically obtained. Next, the actual pressure measurements obtained were discussed and compared to values described by the siphonic siphon design tool. The pressure measurements described are detailed in Figure 32 below, and can be seen as points 1, 1_measured, 2, and 2_measured.

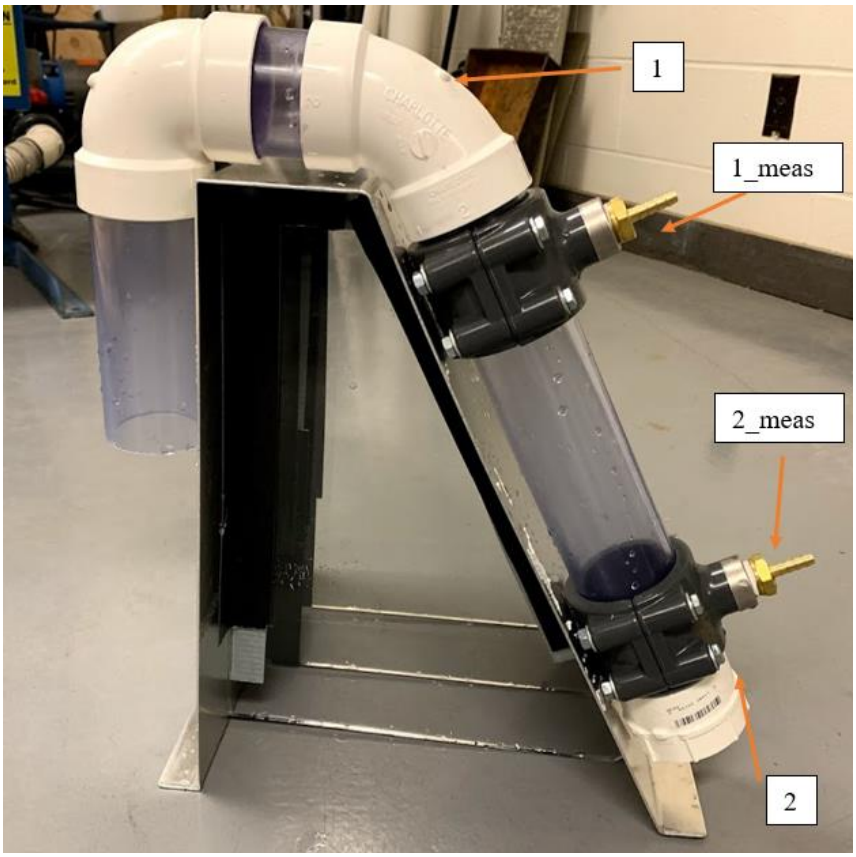

Figure 32: Pressure Location Diagram

Where point 1 is the true concerning upper pressure location within the siphon, otherwise known as point D in the Figure 2. Point 1_meas is the first measured pressure location, which differs from the true concerning point 1 by 11.43 cm [4.5] along the length of the siphon due to sizing constraints of the pipe fittings. Point 2 is the true concerning lower pressure location, prior to entering the lower reservoir, and can be seen as point F in Figure 2. Point 2_meas is the second measured pressure location, which differs from the true concerning point 2 by 8.89 cm [3.5 in] up the length of the siphon due to sizing constraints of the pipe fittings.

5.3.1 Experimental Setup

To obtain the necessary pressure results from the siphon system, the siphon was initially primed. The dam was first mounted within the flume using the mounting screws in the base of

the flume. The edges of the dam were subsequently sealed to the edges of the flume by application of duct tape on all sides. The flume was then turned on at a low flow rate, and the upper reservoir was allowed to fill and overtop at this low flow rate.

The end of the siphon was then subsequently closed using a non-perforated cap. The siphon was placed within the upper reservoir, and allowed to fill completely with water. Once full, the siphon was placed on top of the dam. To more accurately model the siphon hydropower systems used by Rickly, the tailgate was subsequently raised and, a lower reservoir was created to cover the exit of the siphon.

The digital manometer was next calibrated at atmospheric pressure. To obtain pressure readings at the upper pressure location, or point 1_meas, the pressure port of the digital manometer was connected using 4.763 mm [3/16 in] tubing to the upper pressure location (point 1_meas), after being calibrated. The cap at the end of the siphon was subsequently removed, and water was allowed to flow through the siphon, thus beginning siphonic activity. The pump rates were next adjusted to keep the upper reservoir at a steady level, so the majority of the flow would go through the siphon itself, and the weir would not overtop. This flow rate measurement was found through the use of the venturi meter, and subsequently recorded. The upper and lower reservoir depths were subsequently recorded as well. The pressure readings on the digital manometer were allowed to reach a steady state, at which point they were recorded as well. An image of the experimental setup taking pressure readings at the upper pressure location can be seen below, in Figure 33.

Taking pressure readings at the lower pressure location, or point 2_meas, was achieved in a slightly different way. First, the siphonic activity was achieved through a similar fashion as detailed above, without the manometer being connected to the siphon system. Next, the pressure

port of the digital manometer was connected using 4.763 mm [3/16 in] tubing to the lower pressure location (point 2_meas) after being calibrated to the atmosphere. As the pressure at this lower location was theoretically close to or above atmospheric pressure due to the low flow rate through the siphon, the amount of air entrained in the system during the brief period when it was opened to the atmosphere was deemed to be negligible or flushed out quickly. Similarly, pressure readings were obtained once they reached a steady state value.

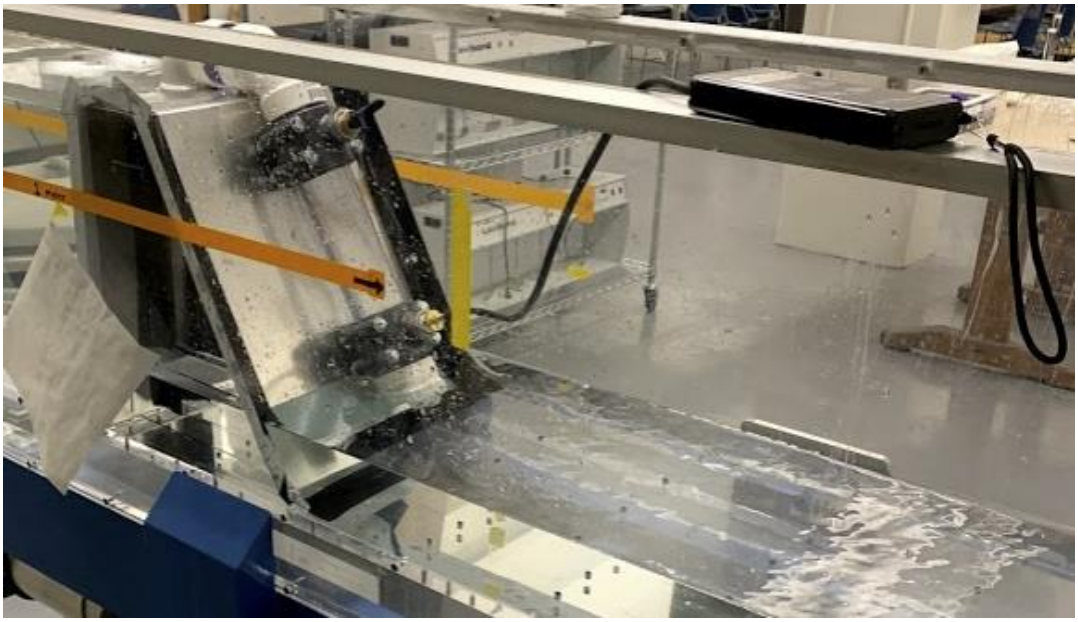

Figure 33: Experimental Setup

When different flow rates were to be analyzed through the use of the two perforated end caps, the siphonic activity was primed as was stated above, at which point the perforated end caps were screwed onto the end of the siphon itself. The pump rates were subsequently adjusted until the upper reservoir reached a steady level again. The upper and lower reservoir depths were recorded for every flow rate as well, and were kept as consistent as possible.

5.3.2 Siphonic Pressure Results

Over the course of the experimentation, 3 different trials were run and subsequent upper and lower pressure values were found using all three different types of flow rates – as such, 9 different data sets were recorded, each containing 2 pressure values. Between each measurement, siphonic activity was stopped and the manometer was disconnected from the siphon system and allowed to return to zero to understand if any error was present within the system. The digital manometer was again calibrated at atmospheric pressure and connected to the siphon in the fashion described above. The siphon was primed again, allowed to reach steady state, and pressure values were recorded. The pressure values displayed would vary over 100 Pa while the siphon was at steady state, and so a median value was selected and recorded.

The recorded flow rate from the venturi meter, as well as the upper and lower reservoir depths were placed into the siphon design tool along with the previously described characteristics to calculate the pressure measurements. As the original siphon design tool would calculate pressure values at the true points of concern – points 1 and 2 in Figure 32 – a second iteration was run within the design tool by adjusting the Bernoulli's equation to calculate the pressure at the experimental locations – points 1_meas and 2_meas. A table of the experimental pressure values at point 1_meas, as well as the calculated pressures at both points 1 and 1_meas for all 9 trials can be seen below, as Table 6. This data can be better visualized in a plot, which can also be seen below, as Figure 34.

Table 6: Pressure Data at Point 1 and Point 1_meas

Trial 1	Flow Rate	Experimental Pressure Point 1_meas (Pa)	Calculated Pressure Point 1 (Pa)	Calculated Pressure Point 1_meas (Pa)
Uncovered	0.104509562	-2934	-3481.52	-1737.86
Coarsely Perforated	0.038161496	-358	-807.75	292.79

Finely Perforated	0.026984253	-40	-591.10	510.41
Trial 2				
Uncovered	0.104509562	-2917	-2708.63	-1737.86
Coarsely Perforated	0.038161496	-368	-647.84	322.93
Finely Perforated	0.026984253	-28	-460.36	510.41
Trial 3				
Uncovered	0.104509562	-2877	-2708.63	-1737.86
Coarsely Perforated	0.038161496	-377	-677.98	292.79
Finely Perforated	0.026984253	-11	-460.36	510.41

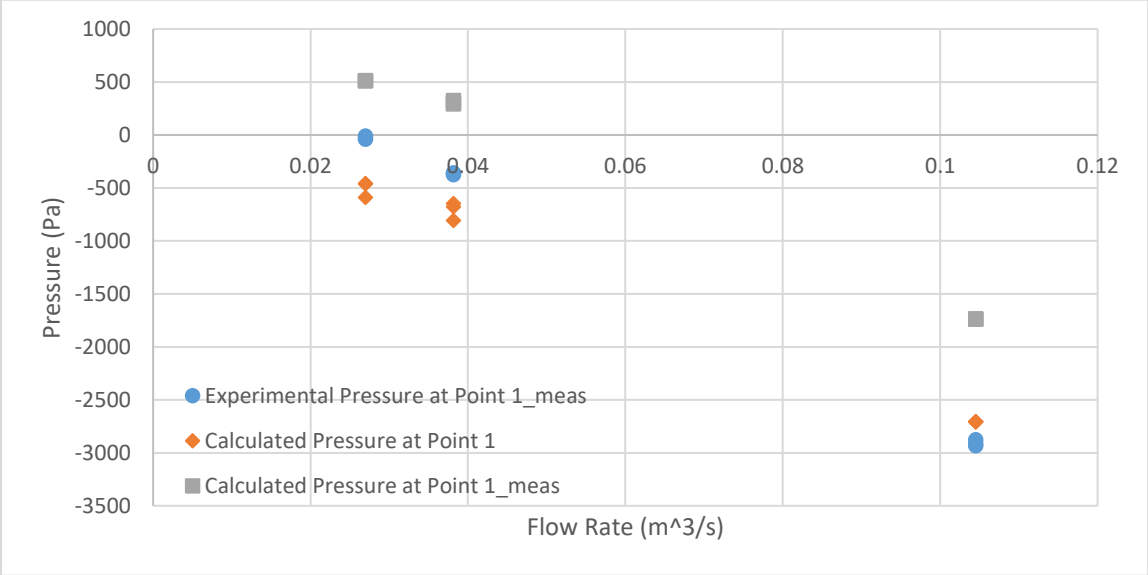

Figure 34: Pressure Data at Point 1 and Point 1_meas

As one can see, the experimentally determined pressure values were similar for all 3 different trials for each flow rate. As well, these values were similar to what was calculated within the siphon design tool. The experimental pressure results at point 1_meas showed a higher pressure than what was calculated for point 1 within the crest, however, this is expected as the results within the siphon should theoretically contain a higher pressure at point 1_meas than at point 1. The experimental results underpredicted what the siphon design tool found when the

siphon design tool was adjusted to take into account the locations where the pressure measurements were taken, or calculated point 1_meas. However, the described error was fairly consistent through all trials except for the highest flow rate, where the error was significantly lower than what was predicted. The error can be explained due to losses found within the piping when the measurements were taken and further air being entrenched within the system when the digital manometers were connected.

In addition to the flow rate measurements taken at the upper pressure location, measurements were also taken at the lower pressure location and can be described below, in Table 7 and Figure 35. Similar to Table 6 and Figure 34, the experimental pressure is measured at point 2_meas, the second critical pressure location within the original generator is seen as point 2 in Figure 32 and as point F in Figure 2, and can be seen as calculated point 2 in Table 7 and Figure 35 below. The calculated pressure when the generator was adjusted to take this difference into consideration is seen as point 2_meas in Figure 32, and as calculated point 2_meas in Table 7 and Figure 35.

Table 7: Pressure Values at Point 2 and Point 2_meas

Trial 1	Flow Rate (m^3/s)	Experimental Pressure Point 2_meas (Pa)	Calculated Pressure Point 2 (Pa)	Calculated Pressure Point 2_meas (Pa)
Uncovered	0.104509562	-938	-1191.32	-1516.67
Coarsely Perforated	0.038161496	175	2035.74	1710.40
Finely Perforated	0.026984253	234	2286.66	2021.10
Trial 2				
Uncovered	0.104509562	-908	-1191.32	-1516.67
Coarsely Perforated	0.038161496	1566	2065.63	1740.29
Finely Perforated	0.026984253	1668	2346.44	2021.10
Trial 3				

Uncovered	0.104509562	-921	-1191.32	-1516.67
Coarsely Perforated	0.038161496	1418	2035.74	1710.40
Finely Perforated	0.026984253	1678	2346.44	2021.10

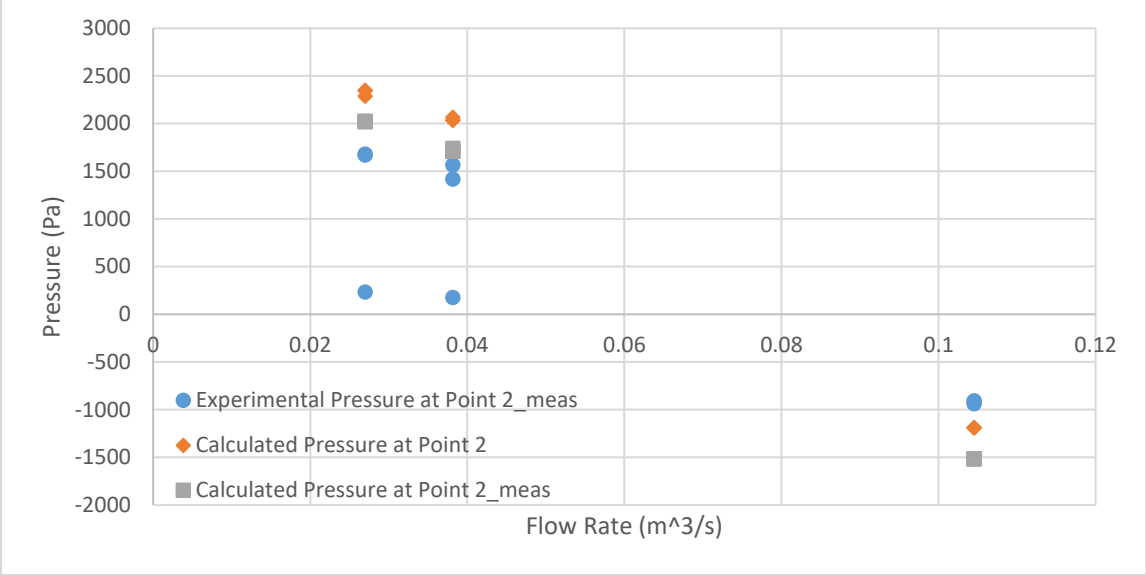

Figure 35: Pressure Data at Point 2 and Point 2_meas

Similarly, the experimental results for most of the values found within the lower pressure location matched similarly. Two of the experimental pressures at point 2_meas – one located at a flow rate of 0.03816 m^3/s and one at a flow rate of 0.02698 m^3/s – for the first trial was severely below what was calculated in the siphon design tool. However, the error in this measurement can be related to erroneously calibrating the digital manometer when taking the reading. As such, these two pressures were not representative of the pressure within the siphon. The rest of the experimental pressure results were much more consistent, and were well within 100 pascals of each other. This being said, there was still some error both between the experimental pressure measurements at point 2_meas and the calculated pressure value at point 2 near the end of the pipe, and the pressure adjusted to match the experimental location (calculated pressure at point 2_meas). While the adjusted pressure calculation from the generator at point 2_meas contained a

lower pressure than the pressure calculated from the generator at point 2, which is expected as it is higher up the body of the siphon, both the calculated pressures at points 2 and 2_meas were lower than the experimental pressure found within the siphon at high flow rates, and greater than the experimental pressure found within the siphon at low flow rates. As well, there seemed to be more error between the experimental and calculated pressure values at high flow rates at both points 2 and 2_meas than there was at lower flow rates. This may be due to the effects viscosity has on the flow at these higher flow rates, and would allow for a greater overall pressure than what was theoretically thought possible. Similar to the upper pressure location, further error can be accounted from entrenched air in the system. The experimental and calculated pressures at lower flow rates at point 2_meas matched fairly well, only varying by several hundred pascals.

As the experimental results matched fairly well to what was produced by the siphon design tool, the design tool was deemed a usable and relatively accurate tool to be used for the design of siphon hydropower systems. The error between the values created by the siphon design tool and those experimentally found were fairly consistent, and can be related to the measurement techniques and viscosity effects within the flow.

One concern is the scalability of the results found through the testing the siphon system. To address this, the Reynolds number for each of the flow rates was tabulated and compared to the Reynolds number of the full scale model, and can be seen below, as Table 8.

Table 8: Experimental and Full Scale Reynolds Numbers

Siphon Type	Flow Rate (m^3/s)	Reynolds Number
Uncovered	0.104509562	5.67E+04
Coarsely Perforated	0.038161496	2.07E+04
Finely Perforated	0.026984253	1.46E+04
Full Scale	1.415840995	3.54E+06

The Reynolds numbers within the experimental setup were much smaller than those found within the real world scenario. While this may be concerning, both Reynolds numbers for the pipe flow throughout the experimental system and within the real world design were well within the turbulent regime, and can be said to be qualitatively similar (Scaling Laws). However, with such a large difference in Reynolds number between the two flows, it can be stated that the experimental design is not completely representative of the flow throughout a real world siphon-turbine system. Further pressure measurements should be recorded at more representative Reynolds numbers to fully validate this siphon design tool, and may be the efforts of future work.

As well, there was a concern of how the major and minor losses within the scale model system compared to the full scale model. As such, the ratio between the major and minor losses experienced throughout the siphon was tabulated and compared to a full scale siphon system, which can be seen below, in Table 9.

Table 9: Major and Minor Losses in Both Full Scale and Model Siphons

Trial	Total Major Losses (m)	Total Minor Losses (m)	Ratio (Major/Minor)
Full Scale	0.237	2.759	0.0858
Uncovered	0.0220	0.250	0.0879
Coarse	0.00369	0.0333	0.111
Fine	0.00201	0.0167	0.121

The ratio of major to minor losses for the full scale siphon system was very similar to that found within the uncovered, coarse, and fine test siphon flow rates. The ratio of major losses to minor losses calculated within the design tool increased as the flow rates decreased, however, this is expected as the chosen diameter was kept as 2 inches within the siphon design tool to be consistent with what was used during the scale model testing. If the design tool was allowed to

select a diameter for this lower flow rate, the ratio of major to minor losses would be more similar to what was found for the full scale and uncovered experiments.

In addition, the flow rates calculated through the venturi meter were compared to the flume manual to better understand whether the high hydrostatic pressure from the dam had a significant effect on the flow rate. The hydrostatic pressure built up behind the dam was 3437.56 Pa [0.5 PSI], or can be seen in head form, as 0.35052 m [1.15 ft]. The experiments were run at 18.5 Hz, 15.1 Hz, and again at 15.1 Hz. While the slowest flow rate used an equivalent pump rate to the medium flow rate, a slower flow rate was measured through the fluid manometers. As the flume manual only presents the pump rates in increments of 5 Hz, the flow rate results within the manual were linearly interpolated from this data. As the results within the flume manual are reported in ft^3/s, they were converted to m^3/s for the sake of this comparison. These results can be seen below, in Table 10.

Table 10: Flow Rate from Manual vs Siphon

Pump Rate	Siphon Flow Rate (m^3/s)	Manual Flow Rate (m^3/s)	Percent Difference
18.5	0.002959378	0.00171597	42.02%
15.1	0.001080612	0.001267896	-17.33%
15.1	0.000764108	0.001267896	-65.93%

It can be seen that that a higher pump rate of 18.5 Hz, the flow throughout the siphon continued to overpredict what was found within the flume manual. However, at low flow rates with high hydrostatic pressure, the flow within the manual seemed to overpredict the flow seen within the siphon, measured by the venturi meter. This is especially seen between the two slowest siphon flow rates, as the measured flow rates were different between these two measured values. The large hydrostatic pressure could have had an effect on the running of the pumps at extremely low pump rates, and when further power is sent to the pump motors, this effect was

negated. The hydrostatic pressure head for these tests were 0.198 m [0.65 ft] higher than the previous tests for flow rate, so this significantly higher pressure head may be the cause of the experimental flow rate underpredicting what was found in manual.

Chapter 6: Conclusion/Future Work

Throughout this work, the design and validation of a siphon hydropower design tool for Rickly Hydropower was investigated. This tool used a variety of inputs to size the siphon system, calculate pressure concerns at several points, and find characteristics on the flow throughout the siphon. The tool was then subsequently validated through the construction of a scale model siphon system within a teaching flume. The tool will be used in the future during the initial design phase of siphon hydropower systems created by Rickly Hydropower. The flow rate of the flume used was also investigated and found using a pitot tube, venturi meter, and sharp crested weir and compared to flow rate values available within the flume manual.

The research contributed to the understanding of siphonic hydropower systems, especially with pressure concerns available at several critical points throughout the siphon. Additionally, the investigation of flow rate measurements can be used to confirm the error of flow rate measurements found within the flume manual, and the accuracy of the venturi meter was directly shown.

6.2 Future Work

In the future, the siphon hydropower design tool should be further validated using a method which more closely matches the Reynolds numbers found in the full scale designs used by Rickly. This may be performed by taking physical pressure measurements at a full scale siphonic hydropower scheme at the two critical pressure locations. Such a test should be performed on a dam whose overall height was near 28 feet, its top width was around 2 feet, its bottom width was around 10 feet, contained an upper reservoir whose depth was around 23 feet, and a lower reservoir whose depth was near 5 feet. As well, it would have a flow rate near 1.42

m^3/s [50 cfs]. These measurements would further validate the tool constructed and discussed above.

The testing for the v-notch weir should be expanded too. As the original tests only used a tape measure to take the fluid depth above the notch measurements, further tests should be performed using a more accurate measurement technique, such as a depth gauge.

As well, further experimentation should be performed to better understand the turbine effects on flow throughout a siphon system. As a reaction turbine incorporates a change in pressure to function, the pressure changes within a siphon due to the turbine being at varying locations should be further studied, and the optimal location for the turbine may be best understood from this.

Finally, further work should be performed in investigating the performance of siphonic hydropower systems. Many of the equations in this tool assumed steady state behavior of the siphon, however, transient processes upon startup and shut done were not explored, as well as headwater and tailwater fluctuations seen throughout the year. These processes should be further understood, and may involve investigation into viscous effects within a siphon. As viscosity has such high effects on the performance of siphonic activity, these effects should be further accounted for within the siphon design tool, and may show that a siphon is able to perform past what is theoretically possible based solely on Bernoulli's principle.

Bibliography

Cengel, Y. A., & Cimbala, J. M. (2006). *Fluid Mechanics: Fundamentals and Applications.* New York, NY: McGraw-Hill.

Chanson, H. (2004). *The Hydraulics of Open Channel Flow: An Introduction.* Elsevier Butterworth-Heinemann.

Coutant, C., Bevelheimer, M. S., & Cada, G. F. (1999). *Technical Evaluation of the Utility of Intake Approach Velocity as an Indicator of Potential Adverse Environmental Impact under Clearn Water Act Section 316(b).* Oak Ridge, Tennessee: Oak Ridge National Laboratory.

Dwyer Instruments. (2015). *Series 477AV Handheld Digital Manometer.* Retrieved from Dwyer Instruments: https://www.dwyer-inst.com/PDF_files/TE_477AV_1.pdf

Gerhart, P. M., Gerhart, A. L., & Hochstein, J. I. (2016). *Munson, Young, and Okiishi's Fundamentals of Fluid Dynamics.* United States: John Wiley and Sons.

Hadjerioua, B., Wei, Y., & Kao, S.-C. (2012). *An Assessment of Energy Potential at.* Oak Ridge, Tennessee: Department of Energy.

International Renewable Energy Agency. (2012, June). Renewable Energy Technologies: Cost Analysis Series. *Hydropower*, pp. 21 - 24.

Kovari, J. (1984). *Chapter 8: Hydraulic Formulas Used in Designing Fish Farms.* Retrieved September 2020, from The Food and Agriculture Organization of the United Nations: http://www.fao.org/3/X5744E/x5744e09.htm#chapter%208.%20hydraulic%20formulas%20used%20in%20designing%20fish%20farms

Malavasi, S., Messa, G., Fratino, U., & Pagano, A. (2012). On the pressure losses through perforated plates. *Flow Measurement and Instrumentation*, 57-66.

Martinez, J. J., Deng, Z. D., Klopries, E.-M., Mueller, R., Titzler, P., Zhou, D., . . . Hansten, A. W. (2018). Characterization of a siphon turbine to accelerate low-head. *Journal of Clearer Production*, 35-42.

Nevers, N. d. (1991). *Fluid Mechanics for Chemical Engineers.* McGraw-Hill.

Potter, A., & Barnes, F. H. (1971). The siphon. *Phys. Educ.*, 362-366.

Scaling Laws. (n.d.). Retrieved from Caltech Particle Theory Group: http://theory.caltech.edu/~kapustin/karandash/scaling.pdf

Stark, B., Ando, E., & Hartley, G. (2010). Modelling and performance of a small siphonic hydropower system. *Renewable Energy*, 2451-2464.

URS Corporation. (2010). *River Reintroduction Into Maureas Swamp: An Assessment of an Alternative Siphon System Intake.* Metairie, LA: URS Corporation.

US Energy Information Administration. (2021, March 5). *What is U.S electricity generation by energy source?* Retrieved from U.S Energy Information Administration: https://www.eia.gov/tools/faqs/faq.php?id=427&t=3

Water Power Technologies Office. (n.d.). *Types of Hydropower Plants*. Retrieved from Office of Energy Efficiency and Renewable Energy: https://www.energy.gov/eere/water/types-hydropower-plants

Zhou, D., Gui, J., Deng, Z. D., Chen, H., Yu, Y., Yu, A., & Yang, C. (2019). Development of an ultra-low head siphon hydro turbine using. *Energy*, 43-50.